

Trapped-ion quantum simulations for condensed-phase chemical dynamics: seeking a quantum advantage

Mingyu Kang^{1,2}, Haggai Nuomin³, Sutirtha N. Chowdhury³, Jonathon L. Yuly⁴, Ke Sun^{1,2}, Jacob Whitlow^{1,5}, Jesús Valdiviezo^{6,7}, Zhendian Zhang³, Peng Zhang³, David N. Beratan^{2,3,8,*}, and Kenneth R. Brown^{1,2,3,5,+}

¹Duke Quantum Center, Duke University, Durham, NC, USA

²Department of Physics, Duke University, Durham, NC, USA

³Department of Chemistry, Duke University, Durham, NC, USA

⁴Lewis-Sigler Institute for Integrative Genomics, Princeton University, Princeton, NJ, USA

⁵Department of Electrical and Computer Engineering, Duke University, Durham, NC, USA

⁶Kenneth S. Pitzer Theory Center, University of California, Berkeley, CA, USA

⁷Department of Chemistry, University of California, Berkeley, CA, USA

⁸Department of Biochemistry, Duke University, Durham, NC, USA

*e-mail: david.beratan@duke.edu

+e-mail: ken.brown@duke.edu

ABSTRACT

Simulating the quantum dynamics of molecules in the condensed phase represents a longstanding challenge in chemistry. Trapped-ion quantum systems may serve as a platform for the analog-quantum simulation of chemical dynamics that is beyond the reach of current classical-digital simulation. To identify a “quantum advantage” for these simulations, performance analysis of both classical-digital algorithms and analog-quantum simulation on noisy hardware is needed. In this Perspective, we make this comparison for the simulation of model molecular Hamiltonians that describe intrinsically quantum models for molecules that possess linear vibronic coupling, comparing the accuracy and computational cost. We describe several simple Hamiltonians that are commonly used to model molecular systems, which can be simulated with existing or emerging trapped-ion hardware. These Hamiltonians may serve as stepping stones toward the use of trapped-ion simulators beyond the reach of classical-digital methods. Finally, we identify dynamical regimes where classical-digital simulations seem to have the weakest performance compared to analog-quantum simulations. These regimes may provide the lowest hanging fruit to exploit potential quantum advantages.

Introduction

Quantum chemistry explores how chemical and physical properties emerge from the quantum mechanical equations of motion. Two ubiquitous challenges face quantum chemistry: (i) characterizing the molecular electronic structure and the corresponding properties of molecules at equilibrium, and (ii) describing the time-evolving dynamics of molecules, often in the condensed phase. For both tasks, the highest accuracy is achieved using the full quantum theory, but the computational cost grows exponentially with system size for the most reliable descriptions. As such, high-accuracy simulations of even modest-sized molecules (tens of atoms) are challenging, even on the world’s finest supercomputers¹⁻³. The most common approach to addressing quantum problems on classical computers is to use approximations. While many practical approximations are available, there is generally a trade-off between accuracy and computational cost.

It was suggested that quantum computers/simulators might provide an advantage over classical-digital simulation for problems faced in quantum chemistry, since quantum properties may be best explored using computational resources that, themselves, are intrinsically quantum mechanical⁴⁻⁶. A quantum advantage could drive scientific progress by providing access to the understanding of quantum phenomena in otherwise inaccessible systems, thus opening up new opportunities in science and engineering. Yet, progress on this path remains an outstanding challenge, not only because of the daunting scientific and engineering challenges of building scalable quantum computers/simulators, but also because of the challenge of discovering how best to exploit the capabilities of (both classical and quantum) simulation tools⁷. A clear “quantum advantage” for a specific quantum computation/simulation over classical-digital simulations for solving a practical problem in quantum chemistry

remains to be proven⁸.

This Perspective motivates the search for a quantum advantage in the area of molecular quantum dynamics^{9–13}, which has received less attention than time-independent (stationary state) quantum chemistry^{14–22}. Even if the full spectrum of electronic and vibrational energies is known, simulating dynamics remains computationally difficult because exact quantum evolution requires tracking evolving phase factors between quantum states, and the number of such phase factors scales exponentially with the system size. Describing the quantum dynamics of molecules, especially for structures in the condensed phase, has the potential to produce valuable insight into a wide variety of chemical, biological, and material phenomena of fundamental and practical value. Advances in understanding the physical underpinnings of photosynthesis^{23,24} and protein function^{25,26} could result from advances in quantum computing and simulations.

Finding quantum advantages requires making detailed comparisons between the strengths and weaknesses of classical-digital and quantum simulation methods. Classical-digital methods, of course, face limitations defined by state-of-art algorithms as well as hardware constraints. Finding opportunities where the performance of quantum simulations may surpass those of classical-digital methods is anticipated to be challenging, as over 80 years of progress in quantum calculations using classical-digital computers must be confronted by an emerging quantum-simulation technology.

At least two quantum-simulation strategies exist: fault-tolerant digital computation and analog simulation. While fault-tolerant digital quantum computation may efficiently solve many problems that are believed to be intractable with classical computers, including quantum molecular dynamics, those solutions require a tremendously large number of operations on a large number of quantum bits (qubits)^{27–30}. These demands are far beyond the capabilities of state-of-art quantum-computing hardware. In the current era of small- or moderate-scale noisy quantum-computing hardware, analog quantum simulation, which exploits the fact that the hardware's native operations are particularly well suited to simulate specific kinds of Hamiltonians, may be considered. The weakness of analog quantum simulation is its inaccuracy, especially when noise is intrinsic to the computing hardware.

Analog quantum simulations have been performed on several platforms, including superconducting structures^{31,32}, neutral-atom assemblies^{33,34}, photonic architectures³⁵, and trapped-ion systems^{36,37}. We focus our attention on trapped-ion systems, which have been used widely for quantum information processing, because of the excellent coherence of their internal states and the availability of high-fidelity state preparation, manipulation, and measurement^{38,39}. As well, significant progress has been made to control the external degrees of freedom for trapped ions, namely their motional modes^{40–45}. The internal and external states of trapped ions can be mapped onto the electronic and nuclear degrees of freedom of molecular Hamiltonians. This makes trapped-ion systems natural candidates for analog quantum simulators of quantum molecular dynamics. Box 1 overviews typical trapped-ion system.

We suggest a path toward identifying models for quantum molecular-dynamics systems that are challenging to address using classical-digital methods, but could be solved using analog simulations on trapped-ion hardware. In this Perspective, we first provide an overview of classical-digital simulation methods and analog trapped-ion simulation approaches for computing the quantum dynamics of molecular Hamiltonians. Then, we compare the performance of the classical-digital and trapped-ion simulations in solving a model problem in quantum dynamics. We discuss parameter regimes where the trapped-ion simulation may provide an advantage. Then, we introduce candidate models of chemical dynamics to explore in the near-term using trapped-ion simulations. Finally, we discuss the outlook for using trapped-ion simulators to address less well-studied challenges in quantum chemistry, and we conclude with a summary of future prospects.

Box 1 | Trapped ions

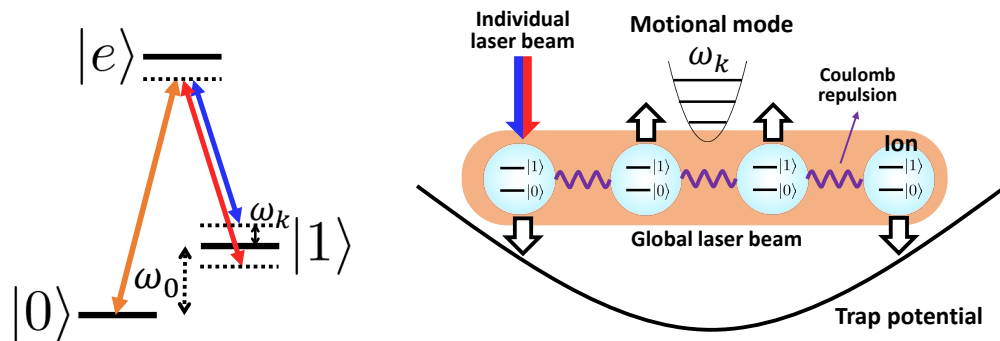
A typical trapped-ion system consists of a linear chain of ions confined in free space. The radio frequency (rf) electromagnetic fields are supplied by the electrodes of the trap, creating a pseudo-potential that constrains the atomic positions. After the ions are sufficiently cooled using lasers, the ions' interactions with the confinement potential and the Coulomb repulsion among the ions reach equilibrium, producing a linear chain of ions.

A typical ion has many accessible electronic states, and two stable states can be exploited to establish an atom-based qubit with near-perfect coherence properties. Initialization of the qubit to a desired state, and measurement of the qubit state, may be performed through optical excitation with lasers.

Nuclear (bosonic) degrees of freedom exist in the ion chain through its collective vibrating motion. The ion chain's motion can be described in the language of normal modes, where each mode is approximated by a quantum harmonic oscillator. An n -ion chain has $3n$ motional modes in total, and n , $2n$, or $3n$ modes can typically be used to interact with the qubits. Such interactions can be used to mediate the entanglement between qubits or to provide the bosonic ingredient for analog simulations. Since the normal modes are spread through the ion chain, each mode can interact with *all* qubits in the chain (except for qubits located at nodes of the normal mode), allowing flexibility in the structure of the Hamiltonians

that can be simulated.

To manipulate the qubit states and motional states of the ion chain, electromagnetic fields are applied using lasers or magnetic field gradients. The figure in the box below shows the example of using lasers to couple the leftmost ion's qubit states to a motional mode. The frequency, phase, and amplitude of the laser fields impinging on each ion can be controlled individually, allowing flexibility in defining the Hamiltonian parameters that will be simulated on the ion chain.



The contenders: classical-digital vs trapped-ion quantum-analog

The current champion: classical-digital simulation methods

Numerical methods to describe quantum dynamics on classical-digital computers are well-established. The quantum nature of molecular systems, and their coupling to the surrounding environment, place the cost of accurate simulations on classical-digital computers out of reach for most systems of interest, as the Hilbert space dimension grows exponentially with the number of degrees of freedom in the simulated system. Thus, sophisticated simulation methods provide access to approximate descriptions of systems' time evolution. There is a trade-off among system size, structure of condensed-phase model, level of approximation, accuracy, and computational cost.

We will discuss some of the challenge of simulating quantum molecular dynamics in the condensed phase using familiar linear vibronic coupling models (LVCs)^{12,46–48}. This class of models is approximate, and real molecules exhibit rich anharmonicities and nonlinear interactions that are beyond the reach of these simple models (see the Outlook section below). A LVC includes M electronic states and N harmonic bath modes, where the bath modes represent the degrees of freedom in the intra/intermolecular vibrations and/or the vibrations of solvents. Each electronic state and the linear coupling between electronic states is often coupled linearly to the bath degrees of freedom. The generic Hamiltonian in second-quantized notation is

$$\hat{H}_{\text{mol}} = \sum_{i,j=1}^M \hat{\psi}_i^\dagger \hat{\psi}_j \left(\frac{\Delta_{i,j}}{2} + \sum_{k=1}^N \kappa_{i,j,k} (\hat{a}_k + \hat{a}_k^\dagger) \right) + \sum_{k=1}^N v_k \hat{a}_k^\dagger \hat{a}_k, \quad (1)$$

where we set $\hbar = 1$ and $\hat{\psi}_i^\dagger$ and $\hat{\psi}_i$ are the creation and annihilation operators for electronic state i , and \hat{a}_k^\dagger and \hat{a}_k are those associated with bath mode k . Also, $\Delta_{i,i} := E_i$ is the energy of state i , and $\Delta_{i,j} = \Delta_{j,i}^*$ ($i \neq j$) is the electronic coupling between states i and j . Attached to each $\hat{\psi}_i^\dagger \hat{\psi}_j$ term is a linear coupling to the bath mode of frequency v_k , where the coupling strength is determined by $\kappa_{i,j,k} = \kappa_{j,i,k}^*$. This LVC is general, in that any pair of states can be coupled and any mode can be coupled to any of the electronic states.

We often follow the dynamics as one electron moves from a prepared donor state to an acceptor state. The initial vibrational states are often assumed to be at thermal equilibrium, often at room temperature T_{room} . Some intramolecular mode frequencies satisfy $\hbar v_k \gg k_B T_{\text{room}}$ in the condensed phase, where k_B is Boltzmann's constant, so that the initial average phonon number of each mode is much less than one. As such, a quantum treatment of these modes is needed.

A simulation method is deemed *numerically exact* if it describes the time evolution of (1) up to a controllable error, which can be made arbitrarily small if infinite computing resources are used. We also define a simulation method to be *approximate* if it relies on a physical or mathematical simplification of the Hamiltonian dynamics, so the method does not converge to the exact solution even given infinite computational resources. We focus on approximations to quantum molecular dynamics that use classical-dynamical heuristics and/or formal expansions of the quantum-mechanical path integral around the classical trajectories of the system (trajectories that satisfy the Lagrange equations of motion).

Assuming that the electronic and vibrational energy states can be obtained, algorithms exist for classical-digital computers to compute numerically exact quantum molecular dynamics in some regimes. Examples include the multi-configuration time-

dependent Hartree (MCTDH) method^{49–51}, the hierarchical equations of motion (HEOM) approach^{52–54}, the quasi-adiabatic propagator path integral (QUAPI) method^{55–61}, the time-evolving matrix products operators (TEMPO) method^{62,63}, and the time-dependent density-matrix renormalization group (tDMRG) method^{64–74}. For example, the tDMRG method can efficiently describe a composite system of electronic states and bath modes when the composite system may be mapped to a one-dimensional chain through an appropriate basis transformation, thus enabling simulations of large systems (e.g., $N \sim 10^3$) with moderate interaction strengths (e.g., $|\kappa_{i,j,k}| \lesssim |\Delta_{i,j}|, |E_i - E_j|, \nu_k$)⁷⁵. However, the tDMRG method is either inaccurate or inefficient when a transformation to a one-dimensional chain cannot be found, or when the interactions are strong (e.g., $|\kappa_{i,j,k}| \sim 10$ to 10^2 times $|\Delta_{i,j}|, |E_i - E_j|, \nu_k$), which is a regime of interest^{76–78}. Other numerically exact methods also become inefficient, in terms of computational time or memory demands, when the entanglement among the components becomes significant^{57,63,79}.

In addition to numerically exact methods, approximate methods may be used to describe quantum dynamics. The much larger mass of nuclei compared to electrons motivates approximate classical or semiclassical descriptions of nuclear motion. Approximations include mean-field strategies, localized classical nuclei, and linearization of quantum propagators. Among the battery of methods, mixed quantum-classical (MQC) and semiclassical (SC) methods may model many features of quantum molecular dynamics, including energy and electron transfer. MQC methods include Ehrenfest dynamics^{80–82}, surface hopping^{83–87}, and mixed quantum-classical Liouville dynamics^{88–93}. The traditional SC approaches include the semiclassical initial value representation (SC-IVR)^{94,95} and linearized SC-IVR (LSC-IVR)^{96,97}. Recently, spin-based methods^{98–101} were also used to simulate nonadiabatic dynamics. In addition to the MQC and SC methods, other imaginary-time path-integral-based trajectory formalisms^{102–111} can provide approximate methods to describe quantum dynamics.

These approximate methods fail when the bath degrees of freedom cannot be treated classically or semi-classically, as when high-frequency vibrations enter. Specifically, many of these approximations may fail to capture detailed balance^{112–114} and lead to the leakage of zero-point energy (ZPE)^{115,116}. One approximate method or another may outperform, depending on the details of the model and the dynamical properties of interest. For example, imaginary-time path-integral-based trajectory approaches may provide quantum dynamics that, despite being approximate, preserve quantum detailed balance and avoids ZPE leakage, thus outperforming traditional SC approaches. However, these trajectory-based methods can be prohibitively computationally expensive^{117,118}.

When the coupling strengths between electronic states and bath modes are weak (e.g., $|\kappa_{i,j,k}| \ll |\Delta_{i,j}|, |E_i - E_j|, \nu_k$), the accuracy of the approximate methods for describing the electronic-state populations over time can be acceptable for timescales that are much shorter than the inverse of the electronic-coupling energy scale (divided by \hbar). Also, when the coupling strengths are extremely strong (e.g., $|\kappa_{i,j,k}| \gg |\Delta_{i,j}|, |E_i - E_j|, \nu_k$), some approximate methods can estimate quantities such as electron-transfer rates well, as semiclassical treatments of harmonic oscillators are often valid for highly excited states. Yet, for many chemical systems between the regimes of weak and strong coupling to bath modes, where quantum entanglement (among electronic states and between electronic states and bath modes) plays a significant role in the time evolution, the approximate methods become inaccurate. In particular, it is difficult to derive an approximation for the quantum dynamics that performs well at both short and long times, although simulating long-time dynamics may be used to determine important quantities, such as equilibrium electronic-state populations¹¹⁹. Therefore, achieving accuracy for longer timescales and for intermediate coupling $|\kappa_{i,j,k}|$ may serve as a compelling target for analog quantum simulations of chemical dynamics.

The upstart: analog trapped-ion simulations

A trapped-ion system allows control over its spin and bosonic degrees of freedom, and thus appears to be a natural platform for performing analog quantum simulations of (quantum) molecular dynamics, as the molecular electronic states can be represented by the spins, and the molecular vibrations can be modeled using the bosonic modes of the trapped-ion system. First, each ion's internal atomic states (spin states) can be used to simulate the electronic states of the LVCM. Typically two of the most stable and readily accessible electronic states are used per ion. As such, a *qubit* is encoded in each trapped ion. It is also possible to encode $d > 2$ states per ion, in which case a *qudit* is encoded^{120,121}. Next, the normal modes associated with ion motion can be used to simulate the bath modes of the LVCM.

Laser or magnetic-field gradients can induce coupling between the ions' electronic states and the motional modes. Each interaction can be mapped to an individual term in the LVCM Hamiltonian, as discussed below. The evolution of the full system to time τ can be simulated using *Trotterization*, where the time evolution of Hamiltonian is simulated for a short time step τ/S , and the process is repeated S times¹⁴. Each evolution with respect to a single Hamiltonian term up to time τ/S can be considered as a “gate”, or a unit of simulation. This is analogous to the way in which quantum computations are typically described using a sequence of gates.

This gate-based analog approach to quantum simulation, also suggested for simulating processes in quantum field theory¹²², contrasts with the traditional approach in analog trapped-ion simulations, where interactions for each and every term in the simulated Hamiltonian are simultaneously switched on^{37,123}. While the traditional approach enabled various quantum-

simulation experiments, even with hardware that does not fully support individual control of qubits (see Ref. 124 for an example of simulating quantum molecular dynamics), the parameters of the simulated Hamiltonian should meet specific constraints¹ that do not exist for the gate-based analog approach.

We now summarize how the LVCM in (1) may be simulated using trapped-ion systems. For simplicity, we consider M ion qubits with N motional modes. In this case, each electronic site is mapped to a qubit, and each bath mode is mapped to a motional mode. For example, an electronic state in which the i^{th} electronic site is occupied and all other sites are unoccupied is represented by the i^{th} qubit at $|1\rangle$ and all other qubits at $|0\rangle$, and the k^{th} bath mode is represented by the ion chain's k^{th} motional mode, where the indices of the ions and motional modes are assigned arbitrarily. We note that when the Hamiltonian has symmetries, it can be simulated using fewer ions, as n ion qubits represent 2^n states¹²⁵. The number of ions can be decreased further when qudits are used rather than qubits¹²⁶.

At the start of a quantum simulation, the trapped-ion qubits are set to states that represent the initial electronic state of the molecule being simulated. For example, the qubit representing an initial electron donor state is set to $|1\rangle$, and all other qubits are set to $|0\rangle$. The motional modes are also cooled to a low-temperature thermal state^{127,128} that represents the initial state of the bath modes in the condensed-phase molecular system. Cooling the motional modes to the ground state is a good approximation when the simulated bath-mode frequencies ν_k satisfy $\hbar\nu_k \gg k_B T_{\text{room}}$.

After initializing the simulation, the time evolution with respect to the LVCM is simulated using trapped ions' native operations that are directly executed by applying electromagnetic fields of appropriate frequencies to the ions. Two of the most widely-used native operations are the single-qubit rotation and the spin-dependent force. First, the single-qubit rotation, which is turned on when the electromagnetic field on ion p is resonant with the qubit frequency ω_0 , is described by the Hamiltonian

$$\hat{H}_p^{(0)} = \frac{\Omega_p}{2} \hat{\sigma}_p^\phi, \quad (2)$$

where $\hat{\sigma}_p^\phi \equiv \hat{\sigma}_p^+ e^{i\phi} + \hat{\sigma}_p^- e^{-i\phi}$, $\hat{\sigma}_p^\pm$ ($\hat{\sigma}_p^\pm$) is the raising (lowering) operator of qubit p , Ω_p is the Rabi frequency of the transition of qubit p , and ϕ is the spin phase determined by the phase of the fields. Next, the spin-dependent force is turned on when the field has two frequencies that are nearly resonant with $\omega_0 + \omega_k$ and $\omega_0 - \omega_k$; we denote these as the blue and red sidebands, respectively, where ω_k is the frequency of motional mode k . When applied to ion p , the Hamiltonian is

$$\hat{H}_{p,k}^{(1)} = \frac{\tilde{\Omega}_{p,k}}{2} \hat{\sigma}_p^\phi \left(\hat{b}_k e^{i[(\mu - \omega_k)t + \varphi]} + h.c. \right) \quad (3)$$

where \hat{b}_k^\dagger (\hat{b}_k) is the creation (annihilation) operator of the resonant mode k , $\tilde{\Omega}_{p,k}$ is the Rabi frequency of the sideband transition of qubit p with respect to mode k , μ (which is nearly resonant with ω_k) is the detuning of the electromagnetic field's frequency from ω_0 , and φ is the motional phase determined by the phase of the fields. We note that the rotating-wave approximation is used to derive both Hamiltonians¹²⁸.

By setting the spin phase ϕ of (2) to 0 $[-\pi/2]$, we can perform single-qubit Pauli-X [Y] rotations $\exp(-i\theta\hat{X}_p/2)$ [$\exp(-i\theta\hat{Y}_p/2)$] by any angle θ , where \hat{X}_p [\hat{Y}_p] is the Pauli-X [Y] operator on qubit p . An arbitrary single-qubit unitary operation, such as a Pauli-Z rotation, can be decomposed into a sequence of Pauli-X and Y rotations¹⁴. This approach enables full control over each individual qubit. Controlling the motion phase φ also allows simulation of the terms $\nu_k \hat{a}_k^\dagger \hat{a}_k$ in (1). This is the case because \hat{H}_{mol} can be re-written in the interaction picture with respect to the bath modes^{71,129,130}, removing the terms $\nu_k \hat{a}_k^\dagger \hat{a}_k$ and converting $\hat{a}_k + \hat{a}_k^\dagger$ to $\hat{a}_k e^{-i\nu_k t} + \hat{a}_k^\dagger e^{i\nu_k t}$, which can be mapped to (3) by appropriately setting φ .

Another important native operation is the Mølmer-Sørensen (MS)^{131,132} interaction, which occurs when a spin-dependent force is applied to two ions p and p' simultaneously. The interaction is described by a Hamiltonian proportional to $\hat{\sigma}_p^\phi \hat{\sigma}_{p'}^{\phi'}$, where ϕ (ϕ') is the spin phase of ion p (p'). While the MS interaction is widely used with quantum-computation gates that generate entanglement between two qubits, we use it here to implement "hopping" transfer (of excitons), to describe the flow of electronic excitation energy between electronic states. The hopping is described by the Hamiltonian

$$\hat{H}_{p,p'}^{(2)} = J(|0\rangle_p |1\rangle_{p'} \langle 1|_p \langle 0|_{p'} + |1\rangle_p |0\rangle_{p'} \langle 0|_p \langle 1|_{p'}) = \frac{J}{2} (\hat{X}_p \hat{X}_{p'} + \hat{Y}_p \hat{Y}_{p'}) = \frac{J}{2} \left(\hat{\sigma}_p^0 \hat{\sigma}_{p'}^0 + \hat{\sigma}_p^{-\pi/2} \hat{\sigma}_{p'}^{-\pi/2} \right). \quad (4)$$

Here, J is determined by the field parameters and time duration of the operation, which are carefully chosen such that there is no residual entanglement between the qubits and the motional modes after the operation^{131,132}. This operation allows the simulation of terms proportional to $\hat{\psi}_i^\dagger \hat{\psi}_j$ in the LVCM for arbitrary pairs of i and j . $\hat{X}_p \hat{X}_{p'}$ and $\hat{Y}_p \hat{Y}_{p'}$ commute, so the two corresponding MS interactions can be implemented sequentially.

¹For example, when a quantum spin system is simulated using the traditional approach where all ions are simultaneously illuminated by a monochromatic beam, the coupling strength $\Delta_{i,j}$ between spins i and j , mapped to ions i and j indexed from the left to right of the ion chain, should satisfy $\Delta_{i,j} \propto |i-j|^{-\alpha}$ ($0 < \alpha < 3$)^{37,123,124}.

Using single-qubit rotation (2), spin-dependent force (3), and hopping (4), each term in (1) can be simulated. Specifically, the terms $E_i \hat{\psi}_i^\dagger \hat{\psi}_i$ are mapped to (2), the terms $\kappa_{i,i,k} \hat{\psi}_i^\dagger \hat{\psi}_i (\hat{a}_k + \hat{a}_k^\dagger)$ are mapped to (3), and the terms $(\Delta_{i,j}/2) \hat{\psi}_i^\dagger \hat{\psi}_j$ ($i \neq j$) are mapped to (4). The terms $\kappa_{i,j,k} \hat{\psi}_i^\dagger \hat{\psi}_j (\hat{a}_k + \hat{a}_k^\dagger)$ ($i \neq j$) are also mapped to a sequence of operations (2)-(4), as described in Ref. 133. The evolution with respect to each term in (1) by the Trotterization time step τ/S is simulated by choosing the field parameters and time duration of each mapped trapped-ion operation appropriately. By repeating the evolution for all terms and Trotterization steps, the evolution of the entire system described by the LVCM Hamiltonian is simulated.

After simulating the system's time evolution, the state of the qubits are measured simultaneously. Each measurement produces a binary result for each ion, reporting whether each ion p was in the state $|0\rangle_p$ or $|1\rangle_p$. Thus, the sequence of cooling, state initialization, time evolution, and measurement needs to be repeated many times to accurately measure the population of each qubit at given point in time. Assuming that experimental measurement error is small (state-of-art measurement error rate for trapped ions^{134,135} is roughly 10^{-4}), the uncertainty of each measured state population is given by $\sqrt{P(1-P)/R}$, where P is the measured population and R is the number of repeated simulation runs. To generate the population curve over S' time steps, the state-population measurement typically needs to be performed separately for each of S' time steps.

The principal benefit of the trapped-ion simulator described above is the favorable scaling of the simulation time with the coupling strengths in the simulated model. As interactions between the molecular components are directly mapped to interactions between the trapped-ion system's components, the required time duration for the trapped-ion simulator's physical operations increases only linearly with the coupling strengths in the LVCM, even in the presence of large entanglements created by strong interactions. The magnitude of noise in the trapped-ion simulator determines the upper limit of the evolution time τ that may be accessed accurately, and this limit may depend on the parameter strengths of the simulated LVCM.

A disadvantage of this quantum analog method is that only limited information of the system's quantum state is revealed by each measurement. Obtaining the full density matrix of the system's state or the bath mode's state⁴⁵ is in principle possible; however, the required number of measurements scales exponentially with the number of qubits or motional modes used¹³⁶. Meanwhile, classical-digital methods such as tDMRG may obtain the full density matrix of the composite state of system and bath modes. In this Perspective, we consider studying the electronic states' population dynamics, as its computational cost is favorable for analog quantum simulations using trapped ions.

Sizing each other up: a test match with a simple model

We now compare the predicted performance of the analog trapped-ion simulation with two classical-digital algorithms, tDMRG and Ehrenfest, by simulating the dynamics of a model Hamiltonian¹³⁷ that is a simple example of a LVCM. The model consists of two electronic states, namely the donor ($|D\rangle$) and acceptor ($|A\rangle$) states, and N bath modes. The Hamiltonian is

$$\hat{H}_{\text{toy}} = \frac{\Delta}{2} (|D\rangle \langle A| + |A\rangle \langle D|) + \sum_{k=1}^N \left[\kappa (|D\rangle \langle D| - |A\rangle \langle A|) (\hat{a}_k + \hat{a}_k^\dagger) + v_k \hat{a}_k^\dagger \hat{a}_k \right], \quad (5)$$

where Δ is the coupling between the two electronic states, v_k is the energy (frequency) of the k -th bath mode, and κ is the state-dependent coupling between the states and each mode. The reorganization energy λ of the system is given by $\lambda = \kappa^2 \sum_{k=1}^N \frac{1}{v_k}$. Typical reorganization energies range from a few Δ to hundreds of Δ ^{138,139}. We assume that the vibrational modes have high frequencies compared to the room temperature (times k_B/\hbar), such that the average phonon number is ~ 0.06 for the initial state of each bath mode in our simulations.

tDMRG simulations are performed by putting (5) into a one-dimensional topology, where the electronic sites and the N bath modes form a linear chain with nearest-neighbor couplings, using the unitary transformation described in Ref. 75. This strategy can be used to describe the dynamics efficiently for a system coupled to a bath with hundreds of modes that have a moderately large reorganization energy ($\lambda \lesssim 10\Delta$). However, the computational cost grows as $\kappa \propto \sqrt{\lambda}$ increases, and as the entanglement among the components grows. In contrast, the Ehrenfest simulations can be performed at significantly lower computation cost than the tDMRG simulations, at the expense of accuracy in describing the dynamics only up to a short time compared to \hbar/Δ , as the semiclassical mean-field approximations often break down at longer times.

We compare the performance of the classical-digital simulations with that of the trapped-ion simulations. Figure 1a shows the population curves for the donor state when $N = 2$, calculated using tDMRG, Ehrenfest, and numerical simulations of the trapped-ion quantum simulation, with various reorganization energy values (λ). To characterize the analog trapped-ion simulations, the evolution of the composite quantum state of the ion qubit and the motional modes is calculated for the specific sequence of pulses, which perform the operations described by (3), that are designed to track the evolution of (5). To model the experimental noise in the trapped-ion simulations, we use Qutip¹⁴⁰ to solve the Lindblad master equation¹⁴¹, which is known to deliver reliable predictions of system performance^{142,143}. We use state-of-art noise parameters¹⁴³⁻¹⁴⁵, which are far from the fundamental limits and can, in principle, be improved.

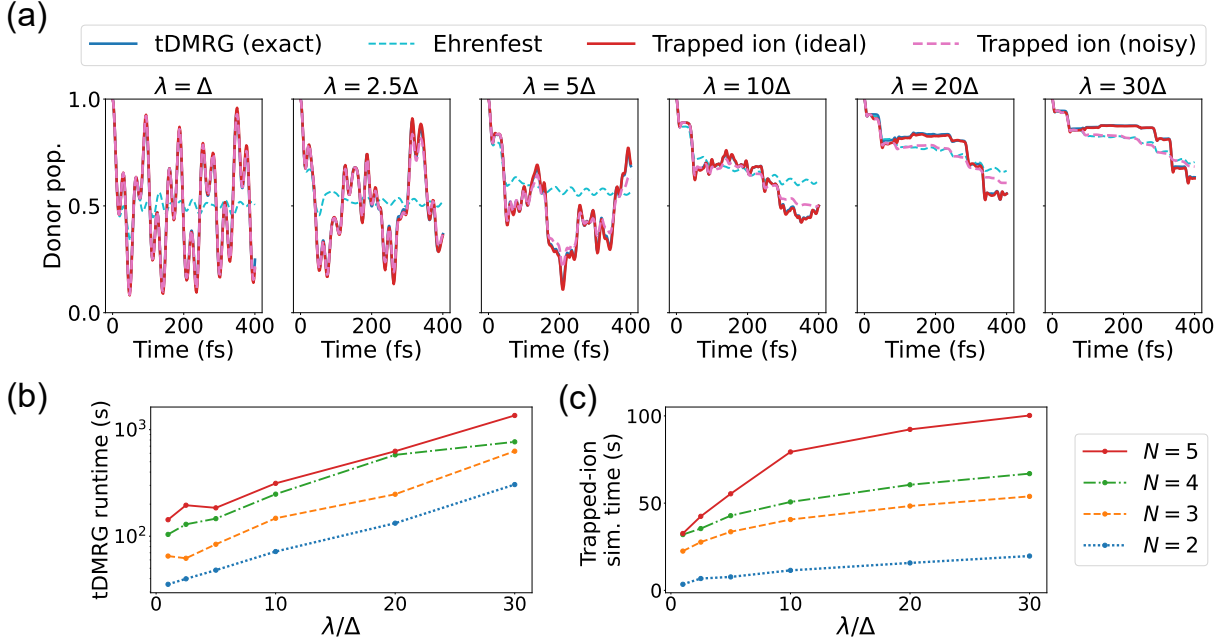


Figure 1. Comparison of classical (tDMRG and Ehrenfest) and quantum (trapped ion) methods for simulating the model Hamiltonian (5). $\Delta = 0.08679$ eV, $v_k = [0.08679 + 0.01240(k - 1)/(N - 1)]$ eV for $k = 1, \dots, N$, where N is the number of bath modes. For the trapped-ion method, we assume using $\lceil N/2 \rceil$ -ion chain to generate N radial motional modes. (a) Evolution of the donor population, for the indicated reorganization energy values (λ) and $N = 2$, simulated using various methods. For the curves labeled “Trapped ion”, we numerically simulate the evolution of a trapped-ion simulator system. The ideal case assumes no decoherence, and the noisy case assumes state-of-art noise parameters, such as the motional heating rate and the coherence times of motional modes and lasers that characterize their dephasing rates². In all panels, the blue and red solid curves overlap. (b) Computational run time for the tDMRG method, with various values of λ/Δ and N . See Ref. 71 for details of the method (the start-geometry algorithm). The singular value decomposition threshold is set to 10^{-4} . Computational run time for the Ehrenfest method is negligible compared to the tDMRG method. (c) Estimated experimental time for the trapped-ion simulation, with various values of λ/Δ and N . We assume 40 equally-spaced time steps and 100 simulation runs per time step, in order to produce accurate estimates of the average donor population from the binary result of each measurement. The time spent for cooling and state preparation, which precedes each simulation, and measurement, which follows each simulation, is not included.

Specifically, we map $|D\rangle$ and $|A\rangle$ to the states $|0\rangle$ and $|1\rangle$ of a single qubit, and use only the spin-dependent force given by (3) that directly simulates the $\kappa(|D\rangle\langle D| - |A\rangle\langle A|)(\hat{a}_k + \hat{a}_k^\dagger)$ terms in an appropriately chosen basis of qubit states. In the interaction picture, the $(\Delta/2)(|D\rangle\langle A| + |A\rangle\langle D|)$ term can be simulated by tuning the spin phase ϕ , similar to the way that $v_k \hat{a}_k^\dagger \hat{a}_k$ terms are simulated by tuning the motional phase φ . In state-of-art trapped-ion systems, the leading sources of errors are heating and dephasing of the motional modes^{142,146}. These errors grow with operation time. Since the physical interaction strength in trapped-ion operations is limited by laser power, simulating (5) with larger $\kappa \propto \sqrt{\lambda}$ requires longer operation times, which reduces the accuracy.

We use N radial motional modes (i.e., in directions perpendicular to the ion chain’s axis) to simulate the bath modes¹⁴⁷. The lasers’ propagation direction needs to be aligned to significantly overlap with these radial directions. We need at least $\lceil N/2 \rceil$ trapped ions to generate N radial motional modes, although operations are performed only on a single qubit that is mapped to the electronic states. We assume that all modes are cooled to zero temperature prior to each simulation run. For the bath-mode frequencies considered here, assuming zero temperature causes negligible error in the computed electronic-state populations.

Even when a spin-dependent force given by (3) is resonant with the sideband frequency of a mode ($\mu = \omega_k$), unwanted off-resonant excitations of other modes, also known as cross-mode coupling, may occur because of the finite spacings between the mode frequencies. Naïvely, this leads to a constraint that $\tilde{\Omega}_{p,k}$ should be much smaller than the mode-frequency spacing,

²For the motional heating rate, we use 5 quanta/s, which is the lowest rate measured in Ref. 144. For the coherence times of motional modes and lasers, we use 36 ms and 500 ms, as measured in Refs. 143 and 145, respectively. The decoherence processes corresponding to these noise parameters are simulated by solving the Lindblad master equation using Qutip¹⁴⁰, following the method in Ref. 143.

which imposes a lower bound on the time duration of the corresponding operations. However, cross-mode coupling can be actively removed by modulating the field parameters during the operation. Here, we consider using a frequency(μ)-modulated pulse^{142, 148, 149} for each spin-dependent-force operation, so that cross-mode coupling is removed using operations with as short a time duration as possible.

For all λ values examined, the populations calculated using the tDMRG and the numerical simulation of the ideal trapped-ion simulation without noise match perfectly. Indeed, both methods capture the quantum dynamics with high accuracy. The Ehrenfest method does not describe the strong population oscillations for smaller values of λ , as the effects of quantum coherence are ignored. The Ehrenfest simulations perform better when the system-bath coupling is very strong ($\lambda \gtrsim 20\Delta$), as the bath oscillators become highly excited and behave nearly classically.

For $\lambda \lesssim 5\Delta$, the populations calculated by the numerical simulation of the noisy trapped-ion simulation closely matches the ideal simulation and the tDMRG analysis, capturing many fine details of the population dynamics. However, for larger λ values, the experimental time approaches the timescale of the noise due to longer operations, so the population curve deviates from the ideal simulation. Interestingly, when λ is very large ($\gtrsim 20\Delta$), the populations of the noisy trapped-ion simulation approach those of the Ehrenfest calculations. This finding suggests a fascinating possibility of mapping certain kinds of semiclassical approximations in chemical dynamics to the effects of the trapped-ion system's experimental noise, possibly allowing a noisy device to approximately simulate an intermediate regime between quantum and semiclassical (e.g., Ehrenfest) chemical dynamics.

Figure 1b and c show the run time of the tDMRG simulation and the experimental time for the trapped-ion simulation, with various λ and N values. For trapped-ion simulation, we assume $S' = 40$ equally-spaced time steps are used to generate the population curve, and $R = 100$ simulation runs are repeated for each time step, which leads to the uncertainty of each measured population P to be $\sqrt{P(1-P)/R} \leq 0.05$ (equal when $P = 0.5$). We note that the lower bound for R required to obtain the state populations within a target accuracy does not depend on the simulated system's size or coupling strengths. The time spent for cooling, state preparation, and measurement, which typically totals a few ms for each simulation run, is excluded from the plotted experimental time.

The run time of the tDMRG simulation increases exponentially with the value of λ . This shows that a model Hamiltonian, even as simple as (5), carries a fairly large computational cost when the entanglement between the molecular components is large. For more complicated models described by (1), where multiple electronic states are strongly coupled to each other and to many vibrational modes, the computation becomes intractable when the entanglement is large. For example, if the Hamiltonian cannot be transformed into a one-dimensional topology, the tDMRG method is inefficient even for systems with moderately large reorganization energy compared to the electronic coupling strength.

The experimental time of the trapped-ion simulations is only $\mathcal{O}(\kappa) = \mathcal{O}(\lambda^{1/2})$. This indicates that trapped ions can simulate strongly entangled dynamics rather efficiently. We expect similar scaling of experimental time to hold for simulations of more complicated models that involve hopping operations given by (4), although hopping may complicate the analysis of accuracy and experimental time, since the total duration of operations that use MS interactions depends on the number of Trotterization steps S^{12} .

Combining (i) the comparison between Fig. 1b and c and (ii) the observation that noisy trapped-ion simulation and Ehrenfest calculation results match for very large λ values, we expect that trapped-ion simulations may have advantages over classical-digital methods, in terms of both computational cost and accuracy, for an *intermediate* regime of reorganization energy compared to the electronic coupling and energy gap. Box 2 provides a general qualitative analysis of the potential advantages of noisy trapped-ion simulation over classical-digital methods for simulating LVCs. The advantages of trapped-ion simulations are expected to be more significant for models that are challenging for classical-digital algorithms, although a more quantitative analysis of the advantages is difficult to make. For example, the coupling strength between different electronic states also affects the run time and accuracy of both classical-digital algorithms and trapped-ion simulations.

Box 2 | LVC: Where might analog trapped-ion simulations win?

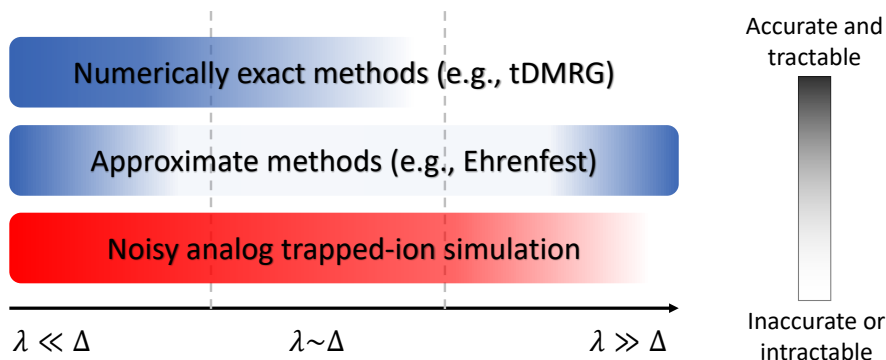
Color gradients in the figure illustrate the qualitative performance (accuracy and computational cost) of three classes of quantum dynamics simulations of LVCs : numerically exact classical-digital methods, approximate classical-digital methods, and analog trapped-ion simulations on a noisy device. The qualitative performance of these methods is illustrated over several regimes of coupling strength between the electronic states and bath modes, quantified by the ratio of the reorganization energy λ to the coupling strength between electronic states Δ .

If $\lambda \ll \Delta$, the numerically exact methods are generally efficient and accurate, since the entanglement between the electronic states and bath modes is weak. In this regime, the approximate methods are also accurate, at least for a few dynamical cycles of the system. This is because the influence of the bath on the electronic states is weak, and

errors associated with neglecting non-classical trajectories of the bath modes have little influence on the evolution of the electronic states.

In the regime where $\lambda \gg \Delta$, the numerically exact methods converge slowly and generally perform poorly because of strong entanglement between the electronic states and bath modes. However, the approximate methods generally perform well, giving good predictions of the donor-state population decay rate, for example. This acceptable performance arises when the coupling is strong and the bath modes are highly-excited harmonic oscillators that often behave almost classically.

In the intermediate regime where $\lambda \sim \Delta$, the coupling can be sufficiently strong that large entanglement renders the numerically exact methods computationally intractable, yet weak enough that the bath modes are not sufficiently highly excited to behave classically. As such, this regime appears to be a compelling target for testing whether an analog trapped-ion simulation may outperform classical-digital algorithms for simulating quantum molecular dynamics economically, at least in the space of LVCMs. The upper bound of λ/Δ that may allow a trapped-ion simulation to produce sufficiently accurate predictions is determined by the magnitude of the noise relative to the strength of native operations of the trapped-ion system.



Candidate models for near-term trapped-ion simulations

To achieve a quantum advantage in simulating LVCMs using analog trapped-ion simulators, it seems best to choose a model with a moderately large number of components strongly coupled to one another, where the couplings have a complex connectivity (when characterized as a graph). Performing accurate quantum simulations of a model of this kind may require trapped-ion simulators that are significantly improved with respect to noise level over state-of-art systems. In this section, we describe three candidate models that can be simulated using current or expected near-term trapped-ion hardware. While each candidate model has a small number of components, each model's dynamics may exhibit signatures of quantum interference and entanglement of interest. Extending these models to larger systems may provide a route toward a quantum advantage in developing simulation tools to understand the complex dynamics of potentially valuable molecular systems.

Conical intersections

The efficient conversion of light into chemical energy plays a central role in the biology of vision¹⁵⁰, DNA damage and repair^{151,152}, and photosynthesis¹³⁸. The underpinning non-adiabatic dynamics typically occur near a conical intersection (CI), or crossing of potential-energy surfaces^{153–155}. Near a CI, the Born-Oppenheimer approximation fails. Thus, a Hilbert space of entangled electronic and nuclear states needs to be considered when considering nonadiabatic dynamics, which increases the memory and computational time required for dynamical simulations.

A quantum-interference effect, known as *geometric phase*, enters the dynamics near CIs^{156–158}. When a wave packet evolves, a time-independent phase accumulates. The phase is path-independent unless a CI is present. When a CI is present, the difference in phase between two pathways depends on the solid angle enclosed by the paths around the CI. This phase can have important effects on the chemical reactions of molecules, even when the nuclei involved have energies well below the energy of the intersection itself^{159,160}.

Consider a model consisting of two electronic states $|D\rangle$ and $|A\rangle$ and two bath modes, labeled x and z :

$$\hat{H}_{\text{CI}} = \kappa_x(|D\rangle\langle A| + |A\rangle\langle D|)(\hat{a}_x + \hat{a}_x^\dagger) + \kappa_z(|D\rangle\langle D| - |A\rangle\langle A|)(\hat{a}_z + \hat{a}_z^\dagger) + \nu_x \hat{a}_x^\dagger \hat{a}_x + \nu_z \hat{a}_z^\dagger \hat{a}_z. \quad (6)$$

The x mode influences the coupling between the electronic states, and the z mode influences the energy splitting between the electronic states¹⁶¹. This Hamiltonian is a simple example of a LVC in (1).

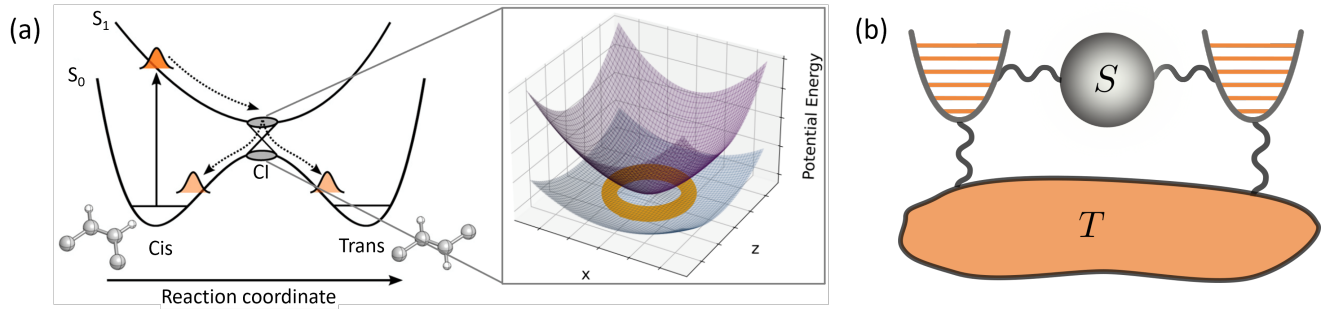


Figure 2. (a) The left panel shows the potential-energy surfaces defined as functions of a reaction coordinate. A conical intersection (CI) occurs when the two potential-energy surfaces cross. A wave packet traveling through the CI displays highly nonadiabatic behavior, including quantum interference between pathways. The center panel illustrates the CI in two dimensions. The mode frequencies and couplings in this example are symmetric, producing degenerate ground states near the CI, as depicted by the orange ring. (b) A schematic representation of the model [see (6)]. The grey sphere, denoted ‘S’, represents the system with two electronic energy levels. The parabola on the left represents a mode that modulates the energy difference of the two levels (i.e., an accepting mode)¹⁶¹. The parabola on the right represents a mode that modulates the coupling strength between the two levels (i.e., a promoting mode)¹⁶¹. The two modes can be coupled to a thermal reservoir of oscillators, denoted ‘T’ [not included in (6)].

Using the Born-Oppenheimer approximation and parameterizing the eigenvector of the electronic subspace in terms of classical nuclear coordinates x , z , p_x , and p_z , where $\xi = \frac{1}{\sqrt{2}}(\hat{a}_\xi + \hat{a}_\xi^\dagger)$ and $p_\xi = \frac{-i}{\sqrt{2}}(\hat{a}_\xi - \hat{a}_\xi^\dagger)$ for $\xi \in \{x, z\}$, the two eigenenergies are $E_\pm = \frac{v_x}{2}(x^2 + p_x^2) + \frac{v_z}{2}(z^2 + p_z^2) \pm \sqrt{2\kappa_x^2 x^2 + 2\kappa_z^2 z^2}$. This choice of basis is referred to as an adiabatic representation, and the associated nuclear potential energies produce a surface for the system to move on adiabatically. The two potential-energy surfaces, in the case of symmetric mode frequencies and couplings ($v_x = v_z$ and $\kappa_x = \kappa_z$), are shown in Fig. 2a, which indicates a CI at the center ($x = z = 0$) and a degenerate ground-state space represented by the orange ring that surrounds the center. The existence of a CI invalidates the Born-Oppenheimer approximation, necessitating a quantum treatment of the full (electronic plus nuclear) dynamics.

Observing the geometric phase, a signature of quantum interference in molecular dynamics, by simulations of (6) with trapped ions was recently proposed^{12,162} and demonstrated experimentally^{163,164}. We note that Ref. 163 uses Trotterization (similar to the scheme described in the previous section), while Ref. 164 uses an approach where the interactions corresponding to every term in (6) are driven simultaneously. Another signature, namely, the wavepacket branching due to a CI, was demonstrated experimentally using a superconducting qubit coupled to electromagnetic cavities¹⁶⁵.

Systems with larger numbers of electronic and vibrational states, as well as multiple CIs, represent a next-level challenge. Adding dissipation, or coupling to a thermal reservoir, mimics more realistic chemical systems of interest, as described in Fig. 2b. While such condensed-phase modeling is beyond the LVCM that has a finite number of bath modes, it provides a potentially more realistic model than the LVCM for describing quantum molecular dynamics. Possible methods of simulating dissipative bath modes are introduced in the Outlook section below. Experimentally isolating and observing the influence of CIs on molecular systems is extremely challenging, so employing analog quantum simulators for simulating models beyond the reach of classical-digital methods may address this challenge.

Vibrationally-assisted energy transfer

Energy transfer in molecular systems, including light-harvesting complexes, occurs in the presence of coupling between chromophores and a bath, defined by protein, solvent, counter-ions, and other species that may be present. The spectral properties of the bath modes, and their coupling strengths, influence the energy-transfer dynamics^{166–171}. Extensive research has addressed how quantum coherence and vibronic dynamics may influence energy-transfer efficiencies in photosynthetic systems^{23,24,172–178}. Understanding the influence of vibrations on quantum coherence and energy transfer may require the study of dynamics in systems where both the electronic and vibrational states are quantized, as in the LVCM.

We now provide an example of a simplified version of the LVCM, which can be readily simulated with trapped-ion systems. The model consists of two electronic states and three bath modes¹⁷⁹. The Hamiltonian is

$$\hat{H}_{\text{VAET}} = (E_A - E_D)|A\rangle\langle A| + \frac{\Delta}{2}(|D\rangle\langle A| + |A\rangle\langle D|) + \sum_{k=1}^2 \kappa_{D,k}|D\rangle\langle D|(\hat{a}_k + \hat{a}_k^\dagger) + \sum_{k=2}^3 \kappa_{A,k}|A\rangle\langle A|(\hat{a}_k + \hat{a}_k^\dagger) + \sum_{k=1}^3 v_k \hat{a}_k^\dagger \hat{a}_k, \quad (7)$$

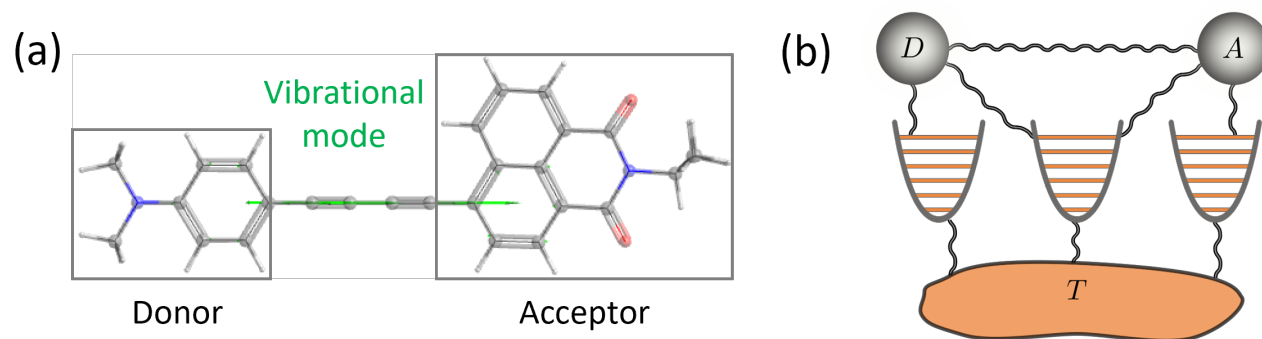


Figure 3. (a) Illustration of a molecular donor-acceptor energy transfer system with intramolecular vibrations. (b) A schematic representation of the vibrationally assisted energy-transfer model [see (7)]. Each grey circle represents an electronic state and each parabola represents a vibrational mode. The vibrational modes can be coupled to a thermal reservoir of oscillators, denoted ‘T’ [not included in (7)].

where E_i is the energy of state i , Δ is the coupling strength between the two states, ν_k is the frequency of mode k , and $\kappa_{i,k}$ is the coupling strength between occupied state i and mode k . Mode 2 is coupled to *both* states, and is thus a correlated or anti-correlated mode that represents intramolecular vibrations, depending on the relative signs of $\kappa_{D,2}$ and $\kappa_{A,2}$.

One reason to simulate (7) is to determine the relationship between the rate of electronic-energy transfer and the bath-mode frequencies. Certain combinations of ν_k 's may produce constructive (destructive) interference, leading to an increase (decrease) in the transfer rate^{179,180}. Also, the correlated or anti-correlated nature of vibrational modes can profoundly influence the chemical dynamics and reactivity^{177,179,181–183}.

Progress has already been made towards analog quantum simulations of models similar to (7), but in limited regimes. A single-mode version of (7) (with only mode 3) has been simulated experimentally using trapped ions¹⁸⁰. Energy transfer in a similar model where electronic states are coupled to a structured semiclassical bath was also simulated experimentally using many qubits in various platforms, including trapped ions¹²⁴, superconducting qubits¹⁸⁴, and NMR qubits¹²⁵. In these experiments, interactions between the electronic states and the bath are simulated by noise injected to the qubits, rather than by interactions between the qubits and the quantum harmonic oscillators. The differences between the quantum and semiclassical treatment of the bath in the energy-transfer phenomenon are discussed in Ref. 185, and this semiclassical bath may not capture all dynamics of interest in real chemical systems.

To move beyond the simulations of VAET in the limited regimes mentioned above, the primary challenge is to achieve full quantum simulations of models with larger numbers of electronic states and quantum vibrational oscillators, so that the model begins to describe some of the complexities of molecular energy-harvesting complexes, such as the Fenna–Matthews–Olson complex²⁴. For a more realistic description of such molecular systems, the vibrational oscillators can be considered to be dissipative and coupled to a thermal reservoir, so that the energy can flow into the reservoir instead of remaining in the electronic states or a few reaction coordinates.

Polarized-light-induced electron transfer

We now consider a molecular system where an electron may tunnel from one part (atom or molecule) of the system to another. Such electron-transfer phenomenon is crucial to understanding catalysis in biological and chemical systems^{186,187}. Quantum effects may play a central role in the dynamics of the electron transfer¹⁸⁸. The underlying mechanism can be approximately described as linear couplings between the electronic states^{189–193}, with potential additional coupling to the bath modes^{189,193,194}, similarly to the energy-transfer model above.

Specifically, we consider as an example a donor-acceptor system, where an electron may hop between the donor and the acceptor when the donor is in one of its excited states. Multiple excited states of the donor lead to multiple pathways of electron transfer, and the possibility of quantum interference between these pathways. When the excited states of the donor are near degenerate, specific superpositions of the excited states may be prepared for electron transfer by controlling the polarization of light that excites the donor. These controllable superposition states produce interferences that can influence the overall electron-transfer rate from the donor to the acceptor¹⁹².

A simple model that shows the influence of light polarization on the electronic dynamics consists of a ground state $|G\rangle$, two excited states $|D_1\rangle$ and $|D_2\rangle$ in which the electron is localized at the donor, and another excited state $|A\rangle$ in which the electron is localized at the acceptor. The couplings between $|G\rangle$ and $|D_i\rangle$ ($i = 1, 2$), which represent the photo-excitation processes of the

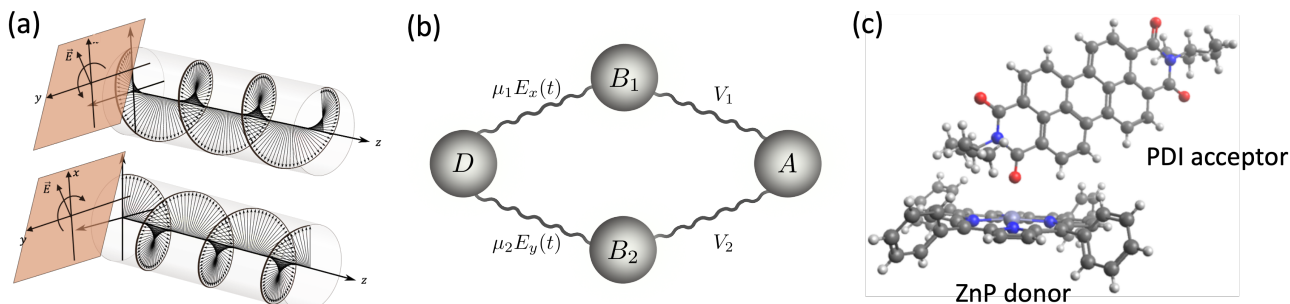


Figure 4. (a) An illustration of left- (top) and right-polarized (bottom) light, to be used to excite a molecular electron donor-acceptor system. (b) A schematic representation of the polarized-light-induced electron-transfer process [see (8)]. In this example $|D_1\rangle$ ($|D_2\rangle$) is polarized in the x (y) direction, such that the x (y) component of the electric field excites $|G\rangle$ to $|D_1\rangle$ ($|D_2\rangle$). Electron transfer occurs from $|D_1\rangle$ and $|D_2\rangle$ to $|A\rangle$. Bath modes are not included in this particular model. (c) An example molecular system (ZnP-PDI), where the polarization of the driving light may influence the electron-transfer rate.

donor molecule, have orthogonal electric-dipole moments $\vec{\mu}_i$ and thus couple differently to the electric field of the driving light. The couplings between $|D_i\rangle$ and $|A\rangle$ represents the electron-transfer processes. The Hamiltonian is given by

$$\hat{H}_{\text{PLET}}(t) = \sum_j \omega_j |j\rangle \langle j| + \sum_{i=1}^2 [\vec{\mu}_i \cdot \vec{E}(t) |G\rangle \langle D_i| + h.c.] + \sum_{i=1}^2 [V_i |D_i\rangle \langle A| + h.c.], \quad (8)$$

where $j = \{G, D_1, D_2, A\}$, ω_j 's are the corresponding energy levels, $\vec{E}(t)$ is the electric field, and V_i is the coupling strength between the state with the donor excited ($|D_i\rangle$) and the state with the electron localized on the acceptor ($|A\rangle$). Bath modes can be straightforwardly added to the Hamiltonian. This model is also a simplified version of the LVCM that can be efficiently simulated using trapped ions. In a recent experiment, the photo-excitation and electron-transfer processes are separately simulated on a trapped-ion qutrit (three-level) system¹²⁶.

The polarization of the driving light affects the population of the two excited donor states and the relative phase between them. Thus, the rate of electron transfer can be controlled by the light polarization. This quantum-interference effect is likely to be diminished when the electronic states' coherence is lost due to coupling to a thermal bath^{189–191}, and may be rich for further exploration. The donor-acceptor model in (8) can also be extended to models of more complex molecular systems with a larger number of excited donor or acceptor states as well as to systems with excitable bridges between the donor and acceptor^{193–197}. Exploring how the driving light and bath modes affect the quantum interference, and eventually the electron-transfer rate in a complex molecular system, is within the LVCM framework and may be a promising avenue for analog trapped-ion simulations.

Outlook: beyond the LVCM

The LVCM offers a simplified framework to investigate molecular quantum dynamics. It is important to note that the LVCM class of Hamiltonians is simple, as (i) it contains only a finite number of vibrational modes that are (ii) harmonic and (iii) only linearly coupled to the electronic states. As a consequence of these simplifications, the LVCM may fail to capture several key aspects of real molecular systems.

For example, the primary vibrational modes that play a crucial role in intermolecular energy transfer are themselves subject to energy dissipation processes, which may arise through interactions with solvent or other vibrational modes. One approach to incorporate dissipation of this kind into simulations is to use a model where the modes that represent nuclear motion are damped by an external reservoir of modes. This external reservoir could represent the solvent and other molecular modes that are orthogonal to the reaction coordinate⁴⁸.

In some approximations^{47,48,198,199} or analytical regimes^{200,201}, a bath consisting of a finite number of damped modes may have the same effects on electronic energy transfer with a bath of infinitely many undamped modes with a continuous (e.g., sum of Lorentzian) spectral density. A bath of continuously distributed modes is different from that described in the LVCM, but is also used widely to study molecule-bath interactions^{47,48,202–207}. For trapped ions, directly simulating a finite number of damped modes is more feasible^{12,199,208} than simulating infinitely many undamped modes, as discussed in the next subsection. Learning appropriate finite-bath approximations for chemical dynamics^{199–201} (or developing approaches to include effectively infinite baths) will be required for the broad applicability of trapped-ion simulations for condensed-phase chemical dynamics.

Aside from the limitations of the LVCM in describing some aspects of chemical dynamics, models beyond the LVCM might provide a compelling target to achieve quantum advantage in simulating molecular dynamics, as the LVCM is a favorable framework for classical-digital simulation. The conceptual and mathematical simplicity of (1), and decades of research into the quantum dynamics of molecules, have led to sophisticated approximation schemes that walk a tightrope between accuracy and computational effort^{54,55,209–215}. There are fundamental reasons to suggest that dynamics generated by the LVCM are particularly well suited for quantum-classical⁹³ or semiclassical^{216,217} analysis using classical computers, as discussed in the next paragraph. Thus, building quantum simulators for models beyond the LVCM may lead to a more immediate quantum advantage, as cutting-edge classical-digital algorithms often rely on the effectiveness of approximations that seem especially suited for the LVCM. Simulating nonlinear system-bath couplings and anharmonic bath modes using trapped ions may require operations that are more challenging to implement than the ones described by (2)-(4) (see the next subsection).

Two examples illustrate the relative effectiveness of quantum-classical and semiclassical approximations for simulating the LVCM. First, the quantum-classical Liouville equations⁸⁸, which approximate open-system quantum dynamics, are exact for the linearly-coupled vibronic dynamics of (1)²¹⁸. Second, in semiclassical theory, the Feynman-Vernon influence functional plays a vital role^{219–222}. Remarkably, the form of this functional is analytic in the limit of a linearly-coupled harmonic bath in (1)²²². This analytic form may then be used instead of numerically calculating the functional. While the quantum-classical Liouville equations and semiclassical approximations based on the Feynman-Vernon influence functional⁶¹ remain difficult to solve, they are computationally less expensive than direct propagation of the time-dependent Schrodinger equation for simulating the LVCM. This suggests that the LVCMs may not be the best target for attempts to achieve a quantum advantage using analog quantum simulations, as the LVCMs constitute a regime of exceptional classical-digital performance.

Analog trapped-ion simulation

There are at least three ways to go beyond the LVCM to describe molecular systems more realistically, and these strategies can make classical-digital simulation methods less tractable (as described in the previous section). First, dissipation of the bath modes may be added. Second, the coupling between electronic states and bath modes may be of higher order, involving terms proportional to $\hat{\psi}_i^\dagger \hat{\psi}_j (\hat{a}_k + \hat{a}_k^\dagger)^n$ where $n \geq 2$ ($n = 2$ corresponds to the quadratic vibronic-coupling model²²³). Third, the bath modes may be anharmonic (fermionic bath modes may exhibit extreme anharmonicity, accommodating only a finite number of states, besides their different statistics from bosons), involving terms proportional to $(\hat{a}_k^\dagger)^n (\hat{a}_k)^n$ where $n \geq 2$.

Trapped ions can be used to simulate all three cases above. First, damping (phonon loss) or heating (phonon gain) of the bath modes can be simulated. Phonon loss can be simulated using laser cooling of the trapped ions' motional modes, such as sideband cooling and electromagnetically induced transparency cooling^{12,199,208}. Laser cooling can be understood as engineered dissipation²²⁴ of the motional modes. The rate of cooling and the final temperature after cooling can be controlled¹²⁷. By interleaving cooling with the usual operations that, by themselves, simulate coherent dynamics of the LVCM, damping of the bath modes during molecular dynamics may be simulated. This may require trapping two kinds of ions, one dedicated to representing electronic states and another dedicated to cooling the motional modes^{225–228}.

Phonon gain also can be similarly simulated by intentionally heating the motional modes, which also requires two kinds of ions²²⁹. Alternatively, phonon gain can be simulated by averaging over many instances of random stochastic operations interleaved with the usual operations for simulating the LVCM. Here, the random stochastic operations are described by (3) with varying amplitude ($\tilde{\Omega}$), phase (φ), and/or detuning (μ) of the laser, which is applied to an auxiliary ion that shares the motional mode. The rate of phonon gain determines the range over which the laser parameters are randomly drawn. This method relies on the fact that evolution with respect to the Lindblad master equation can be realized by an average of many evolutions with respect to a closed system consisting of stochastic Hamiltonian terms^{230,231}. Trapping two kinds of ions is not required with this alternative method. Instead, averaging over a large number of analog-simulation runs may be required in order to achieve a sufficiently low uncertainty in simulating the electronic-state population evolution¹²⁵.

Second, the second-order coupling between electronic states and bath modes can be simulated. Intuitively, as a spin-dependent force (resonant with the first-order sideband $\omega_0 \pm \omega_k$) can be used in simulating a linear coupling that is proportional to $\hat{\psi}_i^\dagger \hat{\psi}_j (\hat{a}_k + \hat{a}_k^\dagger)$, a force resonant with the second-order sideband $\omega_0 \pm \omega_k \pm [\mp] \omega_l$ can be used to simulate a second-order coupling that is proportional to $\hat{\psi}_i^\dagger \hat{\psi}_j (\hat{a}_k \hat{a}_l + \hat{a}_k^\dagger \hat{a}_l^\dagger) [\hat{\psi}_i^\dagger \hat{\psi}_j (\hat{a}_k \hat{a}_l^\dagger + \hat{a}_k^\dagger \hat{a}_l)]$. This was demonstrated in several experiments^{232–237}. A protocol for simultaneously simulating multiple second-order coupling terms is shown in Ref. 238. The challenge in experimental implementations is that the second-order sideband interactions are typically an order of magnitude weaker than the first-order interactions. Thus, larger laser power and/or longer coherence times of the experimental system may be required to simulate the molecular dynamics with second-order vibronic couplings accurately. Similar arguments apply to simulating higher-order vibronic couplings.

Third, the anharmonicity of the bath modes can be simulated. Consider, for example, a model where the anharmonicity $\sum_{k=1}^N \chi_k \hat{a}_k^\dagger \hat{a}_k^\dagger \hat{a}_k \hat{a}_k$ is added to (1), where χ_k is the anharmonicity of mode k . When χ_k is small, one can simulate the Hamiltonian in the interaction picture where the anharmonic term is rotated out and removed, leaving a transformation $\hat{a}_k \rightarrow \hat{a}_k - 2\chi_k \hat{a}_k^\dagger \hat{a}_k \hat{a}_k$

that is valid up to first order in χ_k . This leads to adding weak third-order couplings, which can be simulated as described in the previous paragraph. A general method of simulating anharmonic modes, including the case where the anharmonicity is large, using the motional modes of trapped ions, remains open to further investigation.

Conclusions

In order to identify quantum advantages in simulating molecular quantum dynamics, it is essential to understand the capabilities of both classical-digital algorithms and analog quantum simulations on noisy devices. Using a simplified model Hamiltonian based on linear vibronic couplings, we suggest that analog trapped-ion simulations may have an advantage over classical-digital algorithms, in terms of accuracy and computational cost, in an intermediate regime of coupling strength between the electronic states and bath modes. We present three candidate models relevant to chemical phenomena that can be simulated using current or near-term trapped-ion hardware. In order to achieve a quantum advantage, these models will likely need to be extended to larger sizes, where classical-digital simulations are prohibitively expensive. LVCs with complex connectivity between the electronic states and bath modes, or models where the bath modes are themselves dissipative, are of particular interest. Quantum advantages may also be achieved in models with nonlinear system-bath couplings and anharmonic bath modes, features that semiclassical or quantum-classical approximations struggle to treat accurately.

This Perspective is intended to inspire collaboration between the communities of quantum-chemical theory and analog quantum simulation. Analog quantum simulation may serve as a catalyst for advancing our understanding of complex chemical dynamics, and may allow studying elements of molecular realism that remain inaccessible with current classical-digital simulation approaches.

Acknowledgments

This material is based upon work supported by the Department of Energy under Grant No. DE-SC0019400 (to HN, SNC, JLY, JV, ZZ, and DNB), Grant No. 2127309 to the Computing Research Association for the CIF ellows 2021 Project (to JV), and Grant No. DE-SC0019449 (to KS and JW). In addition, the authors acknowledge the support of the National Science Foundation STAQ Project Phy-181891 (to JW and KRB) and the NSF Quantum Leap Challenge Institute for Robust Quantum Simulation Grant No. OMA-2120757 (to MK, KS, JW, and KRB). JLY acknowledges partial support from the Lewis-Sigler Institute for Integrative Genomics.

References

1. Park, J. W., Al-Saadon, R., MacLeod, M. K., Shiozaki, T. & Vlaisavljevich, B. Multireference electron correlation methods: Journeys along potential energy surfaces. *Chem. Rev.* **120**, 5878–5909 (2020).
2. Park, J. W. & Shiozaki, T. On-the-fly CASPT2 surface-hopping dynamics. *J. Chem. Theory Comput.* **13**, 3676–3683 (2017).
3. Larsson, H. R., Zhai, H., Umrigar, C. J. & Chan, G. K.-L. The chromium dimer: closing a chapter of quantum chemistry. *J. Am. Chem. Soc.* **144**, 15932–15937 (2022).
4. Cirac, J. I. & Zoller, P. Goals and opportunities in quantum simulation. *Nat. physics* **8**, 264–266 (2012).
5. Georgescu, I. M., Ashhab, S. & Nori, F. Quantum simulation. *Rev. Mod. Phys.* **86**, 153 (2014).
6. Daley, A. J. *et al.* Practical quantum advantage in quantum simulation. *Nature* **607**, 667–676 (2022).
7. Alexeev, Y. *et al.* Quantum computer systems for scientific discovery. *PRX Quantum* **2**, 017001 (2021).
8. Lee, S. *et al.* Is there evidence for exponential quantum advantage in quantum chemistry? *arXiv preprint arXiv:2208.02199* (2022).
9. Kassal, I., Jordan, S. P., Love, P. J., Mohseni, M. & Aspuru-Guzik, A. Polynomial-time quantum algorithm for the simulation of chemical dynamics. *Proc. Natl. Acad. Sci.* **105**, 18681–18686 (2008).
10. Sawaya, N. P. *et al.* Resource-efficient digital quantum simulation of d -level systems for photonic, vibrational, and spin- s hamiltonians. *npj Quantum Inf.* **6**, 1–13 (2020).
11. Jahangiri, S., Arrazola, J. M., Quesada, N. & Delgado, A. Quantum algorithm for simulating molecular vibrational excitations. *Phys. Chem. Chem. Phys.* **22**, 25528–25537 (2020).
12. MacDonell, R. J. *et al.* Analog quantum simulation of chemical dynamics. *Chem. Sci.* **12**, 9794–9805 (2021).
13. Saha, D., Iyengar, S. S., Richerme, P., Smith, J. M. & Sabry, A. Mapping quantum chemical dynamics problems to spin-lattice simulators. *J. Chem. Theory Comput.* **17**, 6713–6732 (2021).

14. Nielsen, M. A. & Chuang, I. L. *Quantum Computation and Quantum Information: 10th Anniversary Edition* (Cambridge University Press, USA, 2011), 10th edn.
15. Kitaev, A. Y. Quantum measurements and the Abelian Stabilizer Problem. *Electron. Colloquium Comput. Complex.* **3** (1996).
16. Aspuru-Guzik, A., Dutoi, A. D., Love, P. J. & Head-Gordon, M. Simulated quantum computation of molecular energies. *Science* **309**, 1704–1707 (2005).
17. Lanyon, B. P. *et al.* Towards quantum chemistry on a quantum computer. *Nat. chemistry* **2**, 106–111 (2010).
18. Whitfield, J. D., Biamonte, J. & Aspuru-Guzik, A. Simulation of electronic structure hamiltonians using quantum computers. *Mol. Phys.* **109**, 735–750 (2011).
19. Peruzzo, A. *et al.* A variational eigenvalue solver on a photonic quantum processor. *Nat. communications* **5**, 1–7 (2014).
20. O’Malley, P. J. *et al.* Scalable quantum simulation of molecular energies. *Phys. Rev. X* **6**, 031007 (2016).
21. Kandala, A. *et al.* Hardware-efficient variational quantum eigensolver for small molecules and quantum magnets. *Nature* **549**, 242–246 (2017).
22. Nam, Y. *et al.* Ground-state energy estimation of the water molecule on a trapped-ion quantum computer. *npj Quantum Inf.* **6**, 1–6 (2020).
23. Wang, L., Allodi, M. A. & Engel, G. S. Quantum coherences reveal excited-state dynamics in biophysical systems. *Nat. Rev. Chem.* **3**, 477–490 (2019).
24. Cao, J. *et al.* Quantum biology revisited. *Sci. Adv.* **6**, eaaz4888 (2020).
25. Hammes-Schiffer, S. & Soudackov, A. V. Proton-coupled electron transfer in solution, proteins, and electrochemistry. *The J. Phys. Chem. B* **112**, 14108–14123 (2008).
26. Hammes-Schiffer, S. Proton-coupled electron transfer: Moving together and charging forward. *J. Am. Chem. Soc.* **137**, 8860–8871 (2015).
27. Reiher, M., Wiebe, N., Svore, K. M., Wecker, D. & Troyer, M. Elucidating reaction mechanisms on quantum computers. *Proc. national academy sciences* **114**, 7555–7560 (2017).
28. Babbush, R. *et al.* Encoding electronic spectra in quantum circuits with linear T complexity. *Phys. Rev. X* **8**, 041015 (2018).
29. Su, Y., Berry, D. W., Wiebe, N., Rubin, N. & Babbush, R. Fault-tolerant quantum simulations of chemistry in first quantization. *PRX Quantum* **2**, 040332 (2021).
30. Kim, I. H. *et al.* Fault-tolerant resource estimate for quantum chemical simulations: Case study on Li-ion battery electrolyte molecules. *Phys. Rev. Res.* **4**, 023019 (2022).
31. Houck, A. A., Türeci, H. E. & Koch, J. On-chip quantum simulation with superconducting circuits. *Nat. Phys.* **8**, 292–299 (2012).
32. Hartmann, M. J. Quantum simulation with interacting photons. *J. Opt.* **18**, 104005 (2016).
33. Greiner, M., Mandel, O., Esslinger, T., Hänsch, T. W. & Bloch, I. Quantum phase transition from a superfluid to a mott insulator in a gas of ultracold atoms. *Nature* **415**, 39–44 (2002).
34. Gross, C. & Bloch, I. Quantum simulations with ultracold atoms in optical lattices. *Science* **357**, 995–1001 (2017).
35. Aspuru-Guzik, A. & Walther, P. Photonic quantum simulators. *Nat. physics* **8**, 285–291 (2012).
36. Blatt, R. & Roos, C. F. Quantum simulations with trapped ions. *Nat. Phys.* **8**, 277–284 (2012).
37. Monroe, C. *et al.* Programmable quantum simulations of spin systems with trapped ions. *Rev. Mod. Phys.* **93**, 025001 (2021).
38. Brown, K. R., Kim, J. & Monroe, C. Co-designing a scalable quantum computer with trapped atomic ions. *npj Quantum Inf.* **2**, 1–10 (2016).
39. Bruzewicz, C. D., Chiaverini, J., McConnell, R. & Sage, J. M. Trapped-ion quantum computing: Progress and challenges. *Appl. Phys. Rev.* **6**, 021314 (2019).
40. Kienzler, D. *et al.* Observation of quantum interference between separated mechanical oscillator wave packets. *Phys. review letters* **116**, 140402 (2016).
41. Um, M. *et al.* Phonon arithmetic in a trapped ion system. *Nat. communications* **7**, 1–7 (2016).

42. Zhang, J. *et al.* NOON states of nine quantized vibrations in two radial modes of a trapped ion. *Phys. review letters* **121**, 160502 (2018).
43. Flühmann, C. *et al.* Encoding a qubit in a trapped-ion mechanical oscillator. *Nature* **566**, 513–517 (2019).
44. de Neeve, B., Nguyen, T.-L., Behrle, T. & Home, J. P. Error correction of a logical grid state qubit by dissipative pumping. *Nat. Phys.* **18**, 296–300 (2022).
45. Jia, Z. *et al.* Determination of multimode motional quantum states in a trapped ion system. *Phys. Rev. Lett.* **129**, 103602 (2022).
46. Friesner, R. A. & Silbey, R. Linear vibronic coupling in a general two level system. *The J. Chem. Phys.* **75**, 3925–3936 (1981).
47. Caldeira, A. O. & Leggett, A. J. Quantum tunnelling in a dissipative system. *Annals physics* **149**, 374–456 (1983).
48. Garg, A., Onuchic, J. N. & Ambegaokar, V. Effect of friction on electron transfer in biomolecules. *The J. chemical physics* **83**, 4491–4503 (1985).
49. Lode, A. U., Lévêque, C., Madsen, L. B., Streltsov, A. I. & Alon, O. E. Colloquium: Multiconfigurational time-dependent Hartree approaches for indistinguishable particles. *Rev. Mod. Phys.* **92**, 011001 (2020).
50. Wang, H. & Thoss, M. Multilayer formulation of the multiconfiguration time-dependent Hartree theory. *The J. chemical physics* **119**, 1289–1299 (2003).
51. Meyer, H.-D., Gatti, F. & Worth, G. A. *Multidimensional quantum dynamics: MCTDH theory and applications* (John Wiley & Sons, 2009).
52. Tanimura, Y. Nonperturbative expansion method for a quantum system coupled to a harmonic-oscillator bath. *Phys. Rev. A* **41**, 6676 (1990).
53. Jin, J., Zheng, X. & Yan, Y. Exact dynamics of dissipative electronic systems and quantum transport: Hierarchical equations of motion approach. *J. Chem. Phys.* **128**, 234703 (2008).
54. Yan, Y., Xing, T. & Shi, Q. A new method to improve the numerical stability of the hierarchical equations of motion for discrete harmonic oscillator modes. *J. Chem. Phys.* **153**, 204109 (2020).
55. Kundu, S. & Makri, N. Intramolecular vibrations in excitation energy transfer: Insights from real-time path integral calculations. *Annu. Rev. Phys. Chem.* **73**, 349–375 (2022).
56. Makri, N. Improved Feynman propagators on a grid and non-adiabatic corrections within the path integral framework. *Chem. Phys. Lett.* **193**, 435–445 (1992).
57. Makri, N. Small matrix disentanglement of the path integral: overcoming the exponential tensor scaling with memory length. *J. Chem. Phys.* **152**, 041104 (2020).
58. Makri, N. Small matrix path integral for system-bath dynamics. *J. Chem. Theory Comput.* **16**, 4038–4049 (2020).
59. Makri, N. Small matrix path integral with extended memory. *J. Chem. Theory Comput.* **17**, 1–6 (2020).
60. Makri, N. Small matrix path integral for driven dissipative dynamics. *J. Phys. Chem. A* **125**, 10500–10506 (2021).
61. Topaler, M. & Makri, N. Quasi-adiabatic propagator path integral methods. Exact quantum rate constants for condensed phase reactions. *Chem. physics letters* **210**, 285–293 (1993).
62. Strathearn, A., Kirton, P., Kilda, D., Keeling, J. & Lovett, B. W. Efficient non-markovian quantum dynamics using time-evolving matrix product operators. *Nat. communications* **9**, 3322 (2018).
63. Cygorek, M. *et al.* Simulation of open quantum systems by automated compression of arbitrary environments. *Nat. Phys.* 1–7 (2022).
64. White, S. R. & Feiguin, A. E. Real-time evolution using the density matrix renormalization group. *Phys. review letters* **93**, 076401 (2004).
65. Daley, A. J., Kollath, C., Schollwöck, U. & Vidal, G. Time-dependent density-matrix renormalization-group using adaptive effective hilbert spaces. *J. Stat. Mech. Theory Exp.* **2004**, P04005 (2004).
66. Chin, A. W., Rivas, Á., Huelga, S. F. & Plenio, M. B. Exact mapping between system-reservoir quantum models and semi-infinite discrete chains using orthogonal polynomials. *J. Math. Phys.* **51**, 092109 (2010).
67. Schollwöck, U. The density-matrix renormalization group in the age of matrix product states. *Ann. Phys.* **326**, 96–192 (2011).

68. Chin, A. W., Huelga, S. F. & Plenio, M. B. Chain representations of open quantum systems and their numerical simulation with time-adaptive density matrix renormalisation group methods. In *Semiconductors and Semimetals*, vol. 85, 115–143 (Elsevier, 2011).
69. Del Pino, J., Schröder, F. A., Chin, A. W., Feist, J. & Garcia-Vidal, F. J. Tensor network simulation of polaron-polaritons in organic microcavities. *Phys. Rev. B* **98**, 165416 (2018).
70. Dunnett, A. J. & Chin, A. W. Efficient bond-adaptive approach for finite-temperature open quantum dynamics using the one-site time-dependent variational principle for matrix product states. *Phys. Rev. B* **104**, 214302 (2021).
71. Liu, K. T., Beratan, D. N. & Zhang, P. Improving the efficiency of open-quantum-system simulations using matrix product states in the interaction picture. *Phys. Rev. A* **105**, 032406 (2022).
72. Xie, X. *et al.* Time-dependent density matrix renormalization group quantum dynamics for realistic chemical systems. *J. Chem. Phys.* **151**, 224101 (2019).
73. Liu, K. T., Song, F.-F., Beratan, D. N. & Zhang, P. Suppressing the entanglement growth in matrix product state evolution of quantum systems through nonunitary similarity transformations. *Phys. Rev. B* **106**, 104306 (2022).
74. Xu, Y., Xie, Z., Xie, X., Schollwöck, U. & Ma, H. Stochastic adaptive single-site time-dependent variational principle. *JACS Au* **2**, 335–340 (2022).
75. Prior, J., Chin, A. W., Huelga, S. F. & Plenio, M. B. Efficient simulation of strong system-environment interactions. *Phys. review letters* **105**, 050404 (2010).
76. Miller, J. R., Calcaterra, L. & Closs, G. Intramolecular long-distance electron transfer in radical anions. the effects of free energy and solvent on the reaction rates. *J. Am. Chem. Soc.* **106**, 3047–3049 (1984).
77. Miller, J. R., Beitz, J. V. & Huddleston, R. K. Effect of free energy on rates of electron transfer between molecules. *J. Am. Chem. Soc.* **106**, 5057–5068 (1984).
78. Shibano, Y. *et al.* Large reorganization energy of pyrrolidine-substituted perylene diimide in electron transfer. *The J. Phys. Chem. C* **111**, 6133–6142 (2007).
79. Polyakov, E. A. Real-time motion of open quantum systems: Structure of entanglement, renormalization group, and trajectories. *Phys. Rev. B* **105**, 054306 (2022).
80. Ehrenfest, P. Bemerkung über die angenäherte gültigkeit der klassischen mechanik innerhalb der quantenmechanik. *Zeitschrift fuer Physik* **45**, 455–457 (1927).
81. McLachlan, A. A variational solution of the time-dependent schrodinger equation. *Mol. Phys.* **8**, 39–44 (1964).
82. Agostini, F. & Curchod, B. F. Different flavors of nonadiabatic molecular dynamics. *Wiley Interdiscip. Rev. Comput. Mol. Sci.* **9**, e1417 (2019).
83. Tully, J. C. Molecular dynamics with electronic transitions. *J. Chem. Phys.* **93**, 1061–1071 (1990).
84. Wang, L., Akimov, A. & Prezhdo, O. V. Recent progress in surface hopping: 2011–2015. *J. Phys. Chem. Lett.* **7**, 2100–2112 (2016).
85. Barbatti, M. Nonadiabatic dynamics with trajectory surface hopping method. *Wiley Interdiscip. Rev. Comput. Mol. Sci.* **1**, 620–633 (2011).
86. Subotnik, J. E. *et al.* Understanding the surface hopping view of electronic transitions and decoherence. *Annu. Rev. Phys. Chem.* **67**, 387–417 (2016).
87. Wang, L., Sifain, A. E. & Prezhdo, O. V. Fewest switches surface hopping in Liouville space. *The J. Phys. Chem. Lett.* **6**, 3827–3833 (2015).
88. Kapral, R. & Ciccotti, G. Mixed quantum-classical dynamics. *The J. chemical physics* **110**, 8919–8929 (1999).
89. Mac Kernan, D., Ciccotti, G. & Kapral, R. Trotter-based simulation of quantum-classical dynamics. *The J. Phys. Chem. B* **112**, 424–432 (2008).
90. Kim, H., Nassimi, A. & Kapral, R. Quantum-classical Liouville dynamics in the mapping basis. *J. Chem. Phys.* **129**, 084102 (2008).
91. Hsieh, C.-Y. & Kapral, R. Nonadiabatic dynamics in open quantum-classical systems: Forward-backward trajectory solution. *J. Chem. Phys.* **137**, 22A507 (2012).
92. Hsieh, C.-Y. & Kapral, R. Analysis of the forward-backward trajectory solution for the mixed quantum-classical Liouville equation. *J. Chem. Phys.* **138**, 134110 (2013).

93. Kapral, R. Quantum dynamics in open quantum-classical systems. *J. Physics: Condens. Matter* **27**, 073201 (2015).
94. Miller, W. H. The semiclassical initial value representation: A potentially practical way for adding quantum effects to classical molecular dynamics simulations. *The J. Phys. Chem. A* **105**, 2942–2955 (2001).
95. Miller, W. H. Electronically nonadiabatic dynamics via semiclassical initial value methods. *The J. Phys. Chem. A* **113**, 1405–1415 (2009).
96. Sun, X., Wang, H. & Miller, W. H. Semiclassical theory of electronically nonadiabatic dynamics: Results of a linearized approximation to the initial value representation. *J. Chem. Phys.* **109**, 7064–7074 (1998).
97. Shi, Q. & Geva, E. A relationship between semiclassical and centroid correlation functions. *J. Chem. Phys.* **118**, 8173–8184 (2003).
98. Bossion, D., Ying, W., Chowdhury, S. N. & Huo, P. Non-adiabatic mapping dynamics in the phase space of the $su(n)$ Lie group. *J. Chem. Phys.* **157**, 084105 (2022).
99. Runeson, J. E., Mannouch, J. R., Amati, G., Fiechter, M. R. & Richardson, J. Spin-mapping methods for simulating ultrafast nonadiabatic dynamics. *Chimia* **76**, 582–588 (2022).
100. Runeson, J. E. & Richardson, J. O. Generalized spin mapping for quantum-classical dynamics. *J. Chem. Phys.* **152**, 084110 (2020).
101. Mannouch, J. R. & Richardson, J. O. A partially linearized spin-mapping approach for simulating nonlinear optical spectra. *J. Chem. Phys.* **156**, 024108 (2022).
102. Cao, J. & Voth, G. A. The formulation of quantum statistical mechanics based on the Feynman path centroid density. ii. dynamical properties. *J. Chem. Phys.* **100**, 5106–5117 (1994).
103. Jang, S. & Voth, G. A. A derivation of centroid molecular dynamics and other approximate time evolution methods for path integral centroid variables. *J. Chem. Phys.* **111**, 2371–2384 (1999).
104. Habershon, S., Manolopoulos, D. E., Markland, T. E. & Miller III, T. F. Ring-polymer molecular dynamics: Quantum effects in chemical dynamics from classical trajectories in an extended phase space. *Annu. Rev. Phys. Chem* **64**, 387–413 (2013).
105. Craig, I. R. & Manolopoulos, D. E. Quantum statistics and classical mechanics: Real time correlation functions from ring polymer molecular dynamics. *J. Chem. Phys.* **121**, 3368–3373 (2004).
106. Richardson, J. O. & Thoss, M. Communication: Nonadiabatic ring-polymer molecular dynamics. *J. Chem. Phys.* **139**, 031102 (2013).
107. Ananth, N. Mapping variable ring polymer molecular dynamics: A path-integral based method for nonadiabatic processes. *J. Chem. Phys.* **139**, 124102 (2013).
108. Chowdhury, S. N. & Huo, P. Coherent state mapping ring polymer molecular dynamics for non-adiabatic quantum propagations. *J. Chem. Phys.* **147**, 214109 (2017).
109. Chowdhury, S. N. & Huo, P. State dependent ring polymer molecular dynamics for investigating excited nonadiabatic dynamics. *J. Chem. Phys.* **150**, 244102 (2019).
110. Chowdhury, S. N. & Huo, P. Non-adiabatic Matsubara dynamics and non-adiabatic ring-polymer molecular dynamics. *J. Chem. Phys.* **154**, 124124 (2021).
111. Hele, T. J., Willatt, M. J., Muolo, A. & Althorpe, S. C. Boltzmann-conserving classical dynamics in quantum time-correlation functions: “Matsubara dynamics”. *J. Chem. Phys.* **142**, 134103 (2015).
112. Tully, J. C. *Modern methods for multidimensional dynamics computations in chemistry*, chap. Nonadiabatic Dynamics, 34–72 (World Scientific, 1998).
113. Parandekar, P. V. & Tully, J. C. Mixed quantum-classical equilibrium. *J. Chem. Phys.* **122**, 094102 (2005).
114. Kang, J. & Wang, L.-W. Nonadiabatic molecular dynamics with decoherence and detailed balance under a density matrix ensemble formalism. *Phys. Rev. B* **99**, 224303 (2019).
115. Jain, A. & Subotnik, J. E. Vibrational energy relaxation: A benchmark for mixed quantum–classical methods. *J. Phys. Chem. A* **122**, 16–27 (2018).
116. Persico, M. & Granucci, G. An overview of nonadiabatic dynamics simulations methods, with focus on the direct approach versus the fitting of potential energy surfaces. *Theor. Chem. Acc.* **133**, 1–28 (2014).

117. Ananth, N. Path integrals for nonadiabatic dynamics: Multistate ring polymer molecular dynamics. *Ann. Rev. Phys. Chem.* **73**, 299–322 (2022).
118. Liu, Z., Xu, W., Tuckerman, M. E. & Sun, X. Imaginary-time open-chain path-integral approach for two-state time correlation functions and applications in charge transfer. *J. Chem. Phys.* **157**, 114111 (2022).
119. Bellonzi, N., Jain, A. & Subotnik, J. E. An assessment of mean-field mixed semiclassical approaches: Equilibrium populations and algorithm stability. *J. Chem. Phys.* **144**, 154110 (2016).
120. Low, P. J., White, B. M., Cox, A. A., Day, M. L. & Senko, C. Practical trapped-ion protocols for universal qudit-based quantum computing. *Phys. Rev. Res.* **2**, 033128 (2020).
121. Ringbauer, M. *et al.* A universal qudit quantum processor with trapped ions. *Nat. Phys.* 1–5 (2022).
122. Davoudi, Z., Linke, N. M. & Pagano, G. Toward simulating quantum field theories with controlled phonon-ion dynamics: A hybrid analog-digital approach. *Phys. Rev. Res.* **3**, 043072 (2021).
123. Porras, D. & Cirac, J. I. Effective quantum spin systems with trapped ions. *Phys. review letters* **92**, 207901 (2004).
124. Maier, C. *et al.* Environment-assisted quantum transport in a 10-qubit network. *Phys. Rev. Lett.* **122**, 050501 (2019).
125. Wang, B.-X. *et al.* Efficient quantum simulation of photosynthetic light harvesting. *NPJ Quantum Inf.* **4**, 52 (2018).
126. Sun, K. *et al.* Quantum simulation of polarized light-induced electron transfer with a trapped-ion qutrit system. *arXiv preprint arXiv:2304.12247* (2023).
127. Monroe, C. *et al.* Resolved-sideband raman cooling of a bound atom to the 3D zero-point energy. *Phys. review letters* **75**, 4011 (1995).
128. Wineland, D. J. *et al.* Experimental issues in coherent quantum-state manipulation of trapped atomic ions. *J. research Natl. Inst. Standards Technol.* **103**, 259 (1998).
129. Leibfried, D., Blatt, R., Monroe, C. & Wineland, D. Quantum dynamics of single trapped ions. *Rev. Mod. Phys.* **75**, 281 (2003).
130. Lidar, D. A., Bihary, Z. & Whaley, K. B. From completely positive maps to the quantum Markovian semigroup master equation. *Chem. Phys.* **268**, 35–53 (2001).
131. Mølmer, K. & Sørensen, A. Multiparticle entanglement of hot trapped ions. *Phys. Rev. Lett.* **82**, 1835 (1999).
132. Sørensen, A. & Mølmer, K. Quantum computation with ions in thermal motion. *Phys. review letters* **82**, 1971 (1999).
133. Zhang, J.-N. *et al.* Probabilistic eigensolver with a trapped-ion quantum processor. *Phys. Rev. A* **101**, 052333 (2020).
134. Christensen, J. E., Hucul, D., Campbell, W. C. & Hudson, E. R. High-fidelity manipulation of a qubit enabled by a manufactured nucleus. *npj Quantum Inf.* **6**, 1–5 (2020).
135. Ransford, A., Roman, C., Dellaert, T., McMillin, P. & Campbell, W. C. Weak dissipation for high-fidelity qubit-state preparation and measurement. *Phys. Rev. A* **104**, L060402 (2021).
136. Paris, M. & Rehacek, J. *Quantum state estimation*, vol. 649 (Springer Science & Business Media, 2004).
137. Sato, S. A., Kelly, A. & Rubio, A. Coupled forward-backward trajectory approach for nonequilibrium electron-ion dynamics. *Phys. Rev. B* **97**, 134308 (2018).
138. Ishizaki, A. & Fleming, G. R. Theoretical examination of quantum coherence in a photosynthetic system at physiological temperature. *Proc. Natl. Acad. Sci. U.S.A.* **106**, 17255–17260 (2009).
139. Nitzan, A. *Chemical dynamics in condensed phases: relaxation, transfer and reactions in condensed molecular systems* (Oxford university press, 2006).
140. Johansson, J. R., Nation, P. D. & Nori, F. Qutip: An open-source python framework for the dynamics of open quantum systems. *Comput. Phys. Commun.* **183**, 1760–1772 (2012).
141. Lindblad, G. On the generators of quantum dynamical semigroups. *Commun. Math. Phys.* **48**, 119–130 (1976).
142. Kang, M. *et al.* Designing filter functions of frequency-modulated pulses for high-fidelity two-qubit gates in ion chains. *Phys. Rev. Appl.* **19**, 014014 (2023).
143. Wang, Y. *et al.* High-fidelity two-qubit gates using a microelectromechanical-system-based beam steering system for individual qubit addressing. *Phys. Rev. Lett.* **125**, 150505 (2020).
144. Spivey, R. F. *et al.* High-stability cryogenic system for quantum computing with compact packaged ion traps. *IEEE Transactions on Quantum Eng.* **3**, 1–11 (2021).

145. Zhang, B. *Improving Circuit Performance in a Trapped-Ion Quantum Computer*. Ph.D. thesis, Duke University (2021).
146. Cetina, M. *et al.* Control of transverse motion for quantum gates on individually addressed atomic qubits. *PRX Quantum* **3**, 010334 (2022).
147. Zhu, S.-L., Monroe, C. & Duan, L.-M. Trapped ion quantum computation with transverse phonon modes. *Phys. review letters* **97**, 050505 (2006).
148. Leung, P. H. *et al.* Robust 2-qubit gates in a linear ion crystal using a frequency-modulated driving force. *Phys. review letters* **120**, 020501 (2018).
149. Kang, M. *et al.* Batch optimization of frequency-modulated pulses for robust two-qubit gates in ion chains. *Phys. Rev. Appl.* **16**, 024039 (2021).
150. Polli, D. *et al.* Conical intersection dynamics of the primary photoisomerization event in vision. *Nature* **467**, 440–443 (2010).
151. Barbatti, M. *et al.* Relaxation mechanisms of UV-photoexcited DNA and RNA nucleobases. *Proc. Natl. Acad. Sci.* **107**, 21453–21458 (2010).
152. Matsika, S. Three-state conical intersections in nucleic acid bases. *The J. Phys. Chem. A* **109**, 7538–7545 (2005).
153. Larson, J., Sjöqvist, E. & Öhberg, P. *Conical Intersections in Physics* (Springer, 2020).
154. Yarkony, D. R. Diabolical conical intersections. *Rev. Mod. Phys.* **68**, 985 (1996).
155. Baer, M. *Beyond Born-Oppenheimer: electronic nonadiabatic coupling terms and conical intersections* (John Wiley & Sons, 2006).
156. Ryabinkin, I. G., Joubert-Doriol, L. & Izmaylov, A. F. Geometric phase effects in nonadiabatic dynamics near conical intersections. *Accounts Chem. Res.* **50**, 1785–1793 (2017).
157. Joubert-Doriol, L., Ryabinkin, I. G. & Izmaylov, A. F. Geometric phase effects in low-energy dynamics near conical intersections: A study of the multidimensional linear vibronic coupling model. *J. Chem. Phys.* **139**, 234103 (2013).
158. Li, J., Joubert-Doriol, L. & Izmaylov, A. F. Geometric phase effects in excited state dynamics through a conical intersection in large molecules: N-dimensional linear vibronic coupling model study. *J. Chem. Phys.* **147**, 064106 (2017).
159. Kendrick, B., Hazra, J. & Balakrishnan, N. The geometric phase controls ultracold chemistry. *Nat. communications* **6**, 1–7 (2015).
160. Yuan, D. *et al.* Observation of the geometric phase effect in the $H+HD\rightarrow H_2+D$ reaction. *Science* **362**, 1289–1293 (2018).
161. Lin, S.-H. & Bersohn, R. Effect of partial deuteration and temperature on triplet-state lifetimes. *J. Chem. Phys.* **48**, 2732–2736 (1968).
162. Gambetta, F. M., Zhang, C., Hennrich, M., Lesanovsky, I. & Li, W. Exploring the many-body dynamics near a conical intersection with trapped Rydberg ions. *Phys. Rev. Lett.* **126**, 233404 (2021).
163. Whitlow, J. *et al.* Simulating conical intersections with trapped ions. *arXiv preprint arXiv:2211.07319* (2022).
164. Valahu, C. H. *et al.* Direct observation of geometric phase in dynamics around a conical intersection. *arXiv preprint arXiv:2211.07320* (2022).
165. Wang, C. S. *et al.* Observation of wave-packet branching through an engineered conical intersection. *Phys. Rev. X* **13**, 011008 (2023).
166. Huelga, S. F. & Plenio, M. B. Vibrations, quanta and biology. *Contemp. Phys.* **54**, 181–207 (2013).
167. Adolphs, J. & Renger, T. How proteins trigger excitation energy transfer in the fmo complex of green sulfur bacteria. *Biophys. journal* **91**, 2778–97 (2006).
168. Chin, A. W. *et al.* The role of non-equilibrium vibrational structures in electronic coherence and recoherence in pigment–protein complexes. *Nat. Phys.* **9**, 113–118 (2013).
169. Irish, E., Gómez-Bombarelli, R. & Lovett, B. Vibration-assisted resonance in photosynthetic excitation-energy transfer. *Phys. Rev. A* **90**, 012510 (2014).
170. Nalbach, P., Mujica-Martinez, C. & Thorwart, M. Vibronically coherent speed-up of the excitation energy transfer in the Fenna-Matthews-Olson complex. *Phys. Rev. E* **91**, 022706 (2015).
171. Fujihashi, Y., Fleming, G. R. & Ishizaki, A. Impact of environmentally induced fluctuations on quantum mechanically mixed electronic and vibrational pigment states in photosynthetic energy transfer and 2d electronic spectra. *The J. chemical physics* **142**, 212403 (2015).

172. Engel, G. *et al.* Evidence for wavelike energy transfer through quantum coherence in photosynthetic systems. *Nature* **446**, 782–786 (2007).
173. Christensson, N., Kauffmann, H. F., Pullerits, T. & Mancal, T. Origin of long-lived coherences in light-harvesting complexes. *The J. Phys. Chem. B* **116**, 7449–7454 (2012).
174. Duan, H.-G. *et al.* Nature does not rely on long-lived electronic quantum coherence for photosynthetic energy transfer. *Proc. Natl. Acad. Sci.* **114**, 8493–8498 (2017).
175. Womick, J. M. & Moran, A. M. Vibronic enhancement of exciton sizes and energy transport in photosynthetic complexes. *The J. Phys. Chem. B* **115**, 1347–1356 (2011).
176. Plenio, M. B., Almeida, J. & Huelga, S. F. Origin of long-lived oscillations in 2D-spectra of a quantum vibronic model: electronic versus vibrational coherence. *The J. Chem. Phys.* **139**, 12B614_1 (2013).
177. Tiwari, V., Peters, W. K. & Jonas, D. M. Electronic resonance with anticorrelated pigment vibrations drives photosynthetic energy transfer outside the adiabatic framework. *Proc. Natl. Acad. Sci.* **110**, 1203–1208 (2013).
178. Killoran, N., Huelga, S. F. & Plenio, M. B. Enhancing light-harvesting power with coherent vibrational interactions: A quantum heat engine picture. *The J. chemical physics* **143**, 10B614_1 (2015).
179. Li, Z.-Z., Ko, L., Yang, Z., Sarovar, M. & Whaley, K. B. Unraveling excitation energy transfer assisted by collective behaviors of vibrations. *New J. Phys.* **23**, 073012 (2021).
180. Gorman, D. J. *et al.* Engineering vibrationally assisted energy transfer in a trapped-ion quantum simulator. *Phys. Rev. X* **8**, 011038 (2018).
181. Fassiooli, F., Nazir, A. & Olaya-Castro, A. Quantum state tuning of energy transfer in a correlated environment. *The J. Phys. Chem. Lett.* **1**, 2139–2143 (2010).
182. Sarovar, M., Cheng, Y.-C. & Whaley, K. B. Environmental correlation effects on excitation energy transfer in photosynthetic light harvesting. *Phys. Rev. E* **83**, 011906 (2011).
183. Uchiyama, C., Munro, W. J. & Nemoto, K. Environmental engineering for quantum energy transport. *npj Quantum Inf.* **4**, 1–7 (2018).
184. Potočnik, A. *et al.* Studying light-harvesting models with superconducting circuits. *Nat. communications* **9**, 904 (2018).
185. Li, Z.-Z., Ko, L., Yang, Z., Sarovar, M. & Whaley, K. B. Interplay of vibration-and environment-assisted energy transfer. *New J. Phys.* **24**, 033032 (2022).
186. Marcus, R. A. Chemical and electrochemical electron-transfer theory. *Annu. Rev. Phys. Chem* **15** (1964).
187. Beratan, D. N. Why are dna and protein electron transfer so different? *Annu. Rev. Phys. Chem* **70** (2019).
188. Prytkova, T. R., Kurnikov, I. V. & Beratan, D. N. Coupling coherence distinguishes structure sensitivity in protein electron transfer. *Science* **315**, 622–625 (2007).
189. Skourtis, S. S., Waldeck, D. H. & Beratan, D. N. Inelastic electron tunneling erases coupling-pathway interferences. *The J. Phys. Chem. B* **108**, 15511–15518 (2004).
190. Goldsmith, R. H., Wasielewski, M. R. & Ratner, M. A. Electron transfer in multiply bridged donor- acceptor molecules: dephasing and quantum coherence. *The J. Phys. Chem. B* **110**, 20258–20262 (2006).
191. Zarea, M., Powell, D., Renaud, N., Wasielewski, M. R. & Ratner, M. A. Decoherence and quantum interference in a four-site model system: Mechanisms and turnovers. *The J. Phys. Chem. B* **117**, 1010–1020 (2013).
192. Skourtis, S. S., Beratan, D. N., Naaman, R., Nitzan, A. & Waldeck, D. H. Chiral control of electron transmission through molecules. *Phys. Rev. Lett.* **101** (2008).
193. Xiao, D., Skourtis, S. S., Rubtsov, I. V. & Beratan, D. N. Turning charge transfer on and off in a molecular interferometer with vibronic pathways. *Nano letters* **9**, 1818–1823 (2009).
194. Lin, Z. *et al.* Modulating unimolecular charge transfer by exciting bridge vibrations. *J. Am. Chem. Soc.* **131**, 18060–18062 (2009).
195. Evenson, J. W. & Karpus, M. Effective coupling in bridged electron transfer molecules: computational formulation and examples. *The J. chemical physics* **96**, 5272–5278 (1992).
196. Skourtis, S. S., Beratan, D. N. & Onuchic, J. N. The two-state reduction for electron and hole transfer in bridge-mediated electron-transfer reactions. *Chem. physics* **176**, 501–520 (1993).

197. Troisi, A., Nitzan, A. & Ratner, M. A. A rate constant expression for charge transfer through fluctuating bridges. *The J. chemical physics* **119**, 5782–5788 (2003).
198. Sun, X. & Geva, E. Exact vs. asymptotic spectral densities in the Garg-Onuchic-Ambegaokar charge transfer model and its effect on Fermi's golden rule rate constants. *J. Chem. Phys.* **144**, 044106 (2016).
199. Lemmer, A. *et al.* A trapped-ion simulator for spin-boson models with structured environments. *New J. Phys.* **20**, 073002 (2018).
200. Tamascelli, D., Smirne, A., Huelga, S. F. & Plenio, M. B. Nonperturbative treatment of non-Markovian dynamics of open quantum systems. *Phys. review letters* **120**, 030402 (2018).
201. Mascherpa, F. *et al.* Optimized auxiliary oscillators for the simulation of general open quantum systems. *Phys. Rev. A* **101**, 052108 (2020).
202. Onuchic, J. N., Beratan, D. N. & Hopfield, J. Some aspects of electron-transfer reaction dynamics. *J. Phys. Chem.* **90**, 3707–3721 (1986).
203. Onuchic, J. N. Effect of friction on electron transfer: The two reaction coordinate case. *J. Chem. Phys.* **86**, 3925–3943 (1987).
204. Caldeira, A. O. & Leggett, A. J. Influence of dissipation on quantum tunneling in macroscopic systems. *Phys. Rev. Lett.* **46**, 211 (1981).
205. Caldeira, A. O. & Leggett, A. J. Quantum tunnelling in a dissipative system. *Ann. Phys.* **149**, 374–456 (1983).
206. Leggett, A. Quantum tunneling in the presence of an arbitrary linear dissipation mechanism. *Phys. Rev. B* **30**, 1208 (1984).
207. Leggett, A. J. *et al.* Dynamics of the dissipative two-state system. *Rev. Mod. Phys.* **59**, 1 (1987).
208. Schlawin, F., Gessner, M., Buchleitner, A., Schätz, T. & Skourtis, S. S. Continuously parametrized quantum simulation of molecular electron-transfer reactions. *PRX Quantum* **2**, 010314 (2021).
209. Tanimura, Y. Numerically “exact” approach to open quantum dynamics: The hierarchical equations of motion (HEOM). *J. Chem. Phys.* **153**, 020901 (2020).
210. Zhao, Y., Sun, K., Chen, L. & Gelin, M. The hierarchy of Davydov's Ansatz and its applications. *Wiley Interdiscip. Rev. Comput. Mol. Sci.* **12**, e1589 (2022).
211. Ye, L. *et al.* HEOM-QUICK: a program for accurate, efficient, and universal characterization of strongly correlated quantum impurity systems. *Wiley Interdiscip. Rev. Comput. Mol. Sci.* **6**, 608–638 (2016).
212. Gelin, M. F., Chen, L. & Domcke, W. Equation-of-motion methods for the calculation of femtosecond time-resolved 4-wave-mixing and *n*-wave-mixing signals. *Chem. Rev.* (2022).
213. Ren, J., Li, W., Jiang, T., Wang, Y. & Shuai, Z. Time-dependent density matrix renormalization group method for quantum dynamics in complex systems. *Wiley Interdiscip. Rev. Comput. Mol. Sci.* e1614 (2022).
214. Weimer, H., Kshetrimayum, A. & Orús, R. Simulation methods for open quantum many-body systems. *Rev. Mod. Phys.* **93**, 015008 (2021).
215. De Vega, I. & Alonso, D. Dynamics of non-Markovian open quantum systems. *Rev. Mod. Phys.* **89**, 015001 (2017).
216. Thoss, M. & Wang, H. Semiclassical description of molecular dynamics based on initial-value representation methods. *Annu. Rev. Phys. Chem* **55**, 299 (2004).
217. Lee, M. K., Huo, P. & Coker, D. F. Semiclassical path integral dynamics: Photosynthetic energy transfer with realistic environment interactions. *Annu. Rev. Phys. Chem.* **67**, 639–668 (2016).
218. Mac Kernan, D., Ciccotti, G. & Kapral, R. Surface-hopping dynamics of a spin-boson system. *The J. chemical physics* **116**, 2346–2353 (2002).
219. Makri, N. Feynman path integration in quantum dynamics. *Comput. Phys. Commun.* **63**, 389–414 (1991).
220. Feynman, R. P. & Vernon Jr, F. The theory of a general quantum system interacting with a linear dissipative system. *Ann. Phys.* **281**, 547–607 (2000).
221. Shi, Q. & Geva, E. A derivation of the mixed quantum-classical Liouville equation from the influence functional formalism. *J. Chem. Phys.* **121**, 3393–3404 (2004).
222. May, V. & Kühn, O. *Charge and Energy Transfer Dynamics in Molecular Systems* (John Wiley & Sons, 2011), 3 edn.

223. Zobel, J. P., Heindl, M., Plasser, F., Mai, S. & González, L. Surface hopping dynamics on vibronic coupling models. *Acc. Chem. Res.* **54**, 3760–3771 (2021).
224. Harrington, P. M., Mueller, E. J. & Murch, K. W. Engineered dissipation for quantum information science. *Nat. Rev. Phys.* **4**, 660–671 (2022).
225. Larson, D., Bergquist, J. C., Bollinger, J. J., Itano, W. M. & Wineland, D. J. Sympathetic cooling of trapped ions: A laser-cooled two-species nonneutral ion plasma. *Phys. review letters* **57**, 70 (1986).
226. Blinov, B. *et al.* Sympathetic cooling of trapped Cd^+ isotopes. *Phys. Rev. A* **65**, 040304 (2002).
227. Barrett, M. D. *et al.* Sympathetic cooling of $^9\text{Be}^+$ and $^{24}\text{Mg}^+$ for quantum logic. *Phys. Rev. A* **68**, 042302 (2003).
228. Negnevitsky, V. *et al.* Repeated multi-qubit readout and feedback with a mixed-species trapped-ion register. *Nature* **563**, 527–531 (2018).
229. Clark, C. R., Goeters, J. E., Dodia, Y. K., Viteri, C. R. & Brown, K. R. Detection of single-ion spectra by coulomb-crystal heating. *Phys. Rev. A* **81**, 043428 (2010).
230. Cai, Z. & Barthel, T. Algebraic versus exponential decoherence in dissipative many-particle systems. *Phys. review letters* **111**, 150403 (2013).
231. Chenu, A., Beau, M., Cao, J. & del Campo, A. Quantum simulation of generic many-body open system dynamics using classical noise. *Phys. review letters* **118**, 140403 (2017).
232. Marshall, K. & James, D. F. Linear mode-mixing of phonons with trapped ions. *Appl. Phys. B* **123**, 26 (2017).
233. Shen, Y. *et al.* Quantum optical emulation of molecular vibronic spectroscopy using a trapped-ion device. *Chem. science* **9**, 836–840 (2018).
234. Gan, H., Maslennikov, G., Tseng, K.-W., Nguyen, C. & Matsukevich, D. Hybrid quantum computing with conditional beam splitter gate in trapped ion system. *Phys. review letters* **124**, 170502 (2020).
235. Chen, W., Gan, J., Zhang, J.-N., Matuskevich, D. & Kim, K. Quantum computation and simulation with vibrational modes of trapped ions. *Chin. Phys. B* (2021).
236. Nguyen, C.-H., Tseng, K.-W., Maslennikov, G., Gan, H. & Matsukevich, D. Experimental swap test of infinite dimensional quantum states. *arXiv preprint arXiv:2103.10219* (2021).
237. Chen, W. *et al.* Scalable and programmable phononic network with trapped ions. *Nat. Phys.* 1–7 (2023).
238. Katz, O. & Monroe, C. Programmable quantum simulations of bosonic systems with trapped ions. *arXiv preprint arXiv:2207.13653* (2022).